University of Windsor
Scholarship at UWindsor

Electronic Theses and Dissertations | Theses, Dissertations, and Major Papers

7-17-1969

A study of the bending stresses in a Wildhaber-Novikov gear set.

Omer L. Hageniers
University of Windsor

Follow this and additional works at: https://scholar.uwindsor.ca/etd

Recommended Citation

Hageniers, Omer L., "A study of the bending stresses in a Wildhaber-Novikov gear set." (1969). *Electronic Theses and Dissertations*. 6563.
https://scholar.uwindsor.ca/etd/6563

This online database contains the full-text of PhD dissertations and Masters' theses of University of Windsor students from 1954 forward. These documents are made available for personal study and research purposes only, in accordance with the Canadian Copyright Act and the Creative Commons license—CC BY-NC-ND (Attribution, Non-Commercial, No Derivative Works). Under this license, works must always be attributed to the copyright holder (original author), cannot be used for any commercial purposes, and may not be altered. Any other use would require the permission of the copyright holder. Students may inquire about withdrawing their dissertation and/or thesis from this database. For additional inquiries, please contact the repository administrator via email (scholarship@uwindsor.ca) or by telephone at 519-253-3000ext. 3208.

INFORMATION TO USERS

This manuscript has been reproduced from the microfilm master. UMI films the text directly from the original or copy submitted. Thus, some thesis and dissertation copies are in typewriter face, while others may be from any type of computer printer.

The quality of this reproduction is dependent upon the quality of the copy submitted. Broken or indistinct print, colored or poor quality illustrations and photographs, print bleedthrough, substandard margins, and improper alignment can adversely affect reproduction.

In the unlikely event that the author did not send UMI a complete manuscript and there are missing pages, these will be noted. Also, if unauthorized copyright material had to be removed, a note will indicate the deletion.

Oversize materials (e.g., maps, drawings, charts) are reproduced by sectioning the original, beginning at the upper left-hand corner and continuing from left to right in equal sections with small overlaps.

ProQuest Information and Learning
300 North Zeeb Road, Ann Arbor, MI 48106-1346 USA
800-521-0600

UMI®

Reproduced with permission of the copyright owner. Further reproduction prohibited without permission.

Reproduced with permission of the copyright owner. Further reproduction prohibited without permission.

A STUDY OF THE BENDING STRESSES IN A WILDHABER-NOVIKOV GEAR SET

A Thesis
Submitted to the Faculty of Graduate Studies through the Department of Mechanical Engineering in Partial Fulfilment of the Requirements for the Degree of Master of Applied Science at the University of Windsor

by
Omer L. Hageniers

Windsor, Ontario
1969

Reproduced with permission of the copyright owner. Further reproduction prohibited without permission.

UMI Number:EC52746

UMI®

UMI Microform EC52746
Copyright 2007 by ProQuest Information and Learning Company.
All rights reserved. This microform edition is protected against
unauthorized copying under Title 17, United States Code.

ProQuest Information and Learning Company
789 East Eisenhower Parkway
P.O. Box 1346
Ann Arbor, MI 48106-1346

Reproduced with permission of the copyright owner. Further reproduction prohibited without permission.

ABF0883

APPROVED BY: Thompson

Conant

W North

248700

Reproduced with permission of the copyright owner. Further reproduction prohibited without permission.

ABSTRACT

In this investigation an attempt is made to study the bending stress concentration factor in the Wildhaber Novikov system of gearing. This is done by testing a set of commercially available gears (three dimensional) and a plane model representing the same system (two dimensional study). An equation was developed for the Lewis Factor in this system, based on all the allowable design variables. The objectives of the study also included relating the two dimensional and three dimensional results in a meaningful manner to see if a two dimensional study can produce useful results in a system which employs helical action to transmit motion.

The study of the metal gears involved the use of both photostress on the ends of the teeth and strain gages along their length. The two dimensional study was carried out using a photoelastic approach.

The results of this experiment indicate that the two dimensional bending stress concentration factors can be used to predict the average stress in the three dimensional case. This average stress is independent of where the contact point is along the tooth length (for single tooth contact). It is also necessary to define a stress distribution factor which is the ratio of the maximum stress along the tooth length to the average stress. This stress distribution factor was found to remain constant, for the ratio of axial overlap studied, in the central region of tooth contact. Reasonable comparison was found with previous investigators in terms of the stress concentration factor; however large differences were found in terms of the stress distribution factor.

It is possible to use the photostress technique to determine the locations of maximum bending stress at the end of the tooth. These points agree with those obtained from the two dimensional model. The combination of the three analysis techniques leads to a comprehensive study of a helical gearing system.

Reproduced with permission of the copyright owner. Further reproduction prohibited without permission.

ACKNOWLEDGMENT

I would like to express my thanks to Dr. W. P. T. North for the guidance and encouragement which made this project possible. I would also like to thank the Central Research Shop for the many useful suggestions and workmanship which went into the experimental apparatus.

I would also like to express my thanks to the National Research Council of Canada for their aid in the form of Grant number A3360.

Reproduced with permission of the copyright owner. Further reproduction prohibited without permission.

TABLE OF CONTENTS

Reproduced with permission of the copyright owner. Further reproduction prohibited without permission.

Reproduced with permission of the copyright owner. Further reproduction prohibited without permission.

LIST OF FIGURES

Reproduced with permission of the copyright owner. Further reproduction prohibited without permission.

Reproduced with permission of the copyright owner. Further reproduction prohibited without permission.

NOMENCLATURE

α_ϕ	pressure angle, degrees
a_n	location of apex of inscribed parabola (convex tooth), in.
b	face width, in
β^*	helix angle, degrees
D	circular tooth clearance, in.
δ	cutter clearance angle, degrees
f	load correction factor
F	tooth length (in)
h	concave tooth fillet radius, in.
H	height of Lewis Parabola, in.
K, K_t	stress concentration factor
K_{3-D}	stress concentration factor for three dimensional tooth
K_{2-D}	stress concentration factor for two dimensional tooth
l	profile radius, in.
N	number of teeth
P	contact pressure, lb./in.
P^*	pitch circle correction factor
P	diametral pitch, $in.^{-1}$
P_n	location of apex of inscribed parabola (concave tooth) in.
ψ	angular position variable
ψ_σ	stress distribution factor
ψ_1	angle of offset of pitch point (convex tooth), degrees
ψ_2	angle of offset of pitch point (concave tooth), degrees
R_1	convex gear radius, in.
R_2	concave gear radius, in.
r_f	convex tooth fillet radius, in.
S_1	convex circular tooth thickness, in.
S_2	concave circular tooth thickness, in.
T	thickness of critical tooth section, in.
W_n	normal tooth load, lb.
W_t	tangential tooth load, lb.
χ	tooth length variable

Reproduced with permission of the copyright owner. Further reproduction prohibited without permission.

Y_n Lewis Factor

σ stress, psi

$\bar{\sigma}$ average stress along tooth length

Reproduced with permission of the copyright owner. Further reproduction prohibited without permission.

1. INTRODUCTION

1.1 Subject of Investigation

The purpose of this experiment is to obtain bending stress concentration information for the Novikov system of gearing. A comparison of the stresses in a two dimensional model and a three dimensional gear set will be compared to see if the two dimensional results can be extended to predict the three dimensional bending stresses. The stress concentration data will be presented in a form suitable for design. A generalized expression of the Lewis Form Factor for the Novikov system of gearing will be presented for use in design work.

1.2 Importance of Stress Concentration Information

Two important considerations in gear design are bending strength and surface durability. In order to have an optimum use of material in a system, these two considerations should be balanced into an equal strength system. The surface durability is governed by the contact stresses set up between the gear teeth. The contact stresses can be reasonably predicted by employing a modification of the Hertz contact stress formula (1) (2) (3) (4) (5) (6). However, in the consideration of the bending stresses, no theory is available which accurately predicts these stresses and experimentation must be employed to obtain usable information. The stress concentration factor is then obtained by comparing these stresses to a nominal stress value which is suitable for design.

1.3 Plan of Investigation

The stress distribution on the ends of the gears was studied by employing a photoelastic coating and a reflection polariscope. Based on the results of this study, strain gages were placed along the length of the teeth and strain recordings made. In addition, a two dimensional photoelastic model was constructed corresponding to a normal section through the gears and this model was tested in a polariscope.

Reproduced with permission of the copyright owner. Further reproduction prohibited without permission.

2. LITERATURE REVIEW

2.1 Development of the Wildhaber-Novikov Gear System

The Wildhaber-Novikov, or Circarc gearing system was first developed to provide a gearing system with better contact properties than those shown by the involute system. This is accomplished by making the tooth profiles circular arcs; with one gear having teeth with convex profiles and the mating gear concave profiles. It is immediately evident that this system will have low contact stresses because of the high degree of conformity present. However, this tooth form is not conjugate and must rely on helical action to provide uniform motion.

A system of gearing employing circular arc profiles was first presented by Ernest Wildhaber in 1923 (7) (8). However, subsequent tests on a set of gears proved no great improvement over the involute system and the Circarc gearing was not further developed.

However in 1954 the Circarc system was rediscovered by Col. M. L. Novikov and subsequent investigation and testing showed a large improvement over the involute system. This system has since received wide acceptance in Russia (5).

Then in 1959, Associated Electrical Industries in England began research on, and production of Circarc gears. They found an improvement of 3.8 to 6.5 in load carrying capacity over comparable involute gears (9) (10).

2.2 Stress Analysis

The analysis of gear tooth stressing is very complex and for that reason a great number of assumptions are necessary. The most complete study of Novikov gear tooth stressing in bending is by Fedyakin and Chesnokov (4) (5). In their analysis they first consider the profile as a two dimensional problem and construct the Lewis Parabola graphically to obtain the two dimensional stress. Then loading factors are applied to this in order to correct for the fact that loading is confined to a small area on the face of the tooth (see figure 1). The problem of load distribution in helical gear teeth is discussed more fully by Wellauer and Seireg (11), who apply their

Reproduced with permission of the copyright owner. Further reproduction prohibited without permission.

results to the Novikov system. Some photoelastic results are presented by Allan (2) and Klein (1), but there is not sufficient information given to determine a stress concentration factor. A discussion on the design of Novikov profiles is given by Kaluzhnikov (12), Davis (13), Walker (14), Wells (15), Kugimiya (16), and Johnson(17).

Reproduced with permission of the copyright owner. Further reproduction prohibited without permission.

3. PROBLEM AS STUDIED

3.1 Details of Gears Tested

The gears were supplied by Associated Electrical Industries Limited. The pinion teeth were convex and the wheel teeth concave. Further details are:

Diametral Pitch	5
Helix Angle	23.07°
Number of Teeth: Pinion	17
Number of Teeth: Wheel	29
Pressure Angle (nominal)	25°
Pinion Profile Radius	.4084 inches
Axial Pitch	1.6031 inches
Face Width	2.00 inches
Axial Overlap Ratio	1.25

The gears were fabricated of plain carbon steel and were not heat treated but left in the machined state. Hardness tests were carried out on the gears to obtain further properties. The Brinell hardness of the pinion is 179 and for the wheel it is 151.

3.2 Theoretical Considerations

3.2.1 The Lewis Form Factor: The Lewis Form Factor was one of the first attempts to predict the bending strength of gear teeth. In spite of the fact that it has been proven to be in error with regard to both magnitude and location of the maximum stresses in a gear tooth, it is still used as a basis for gear design. Since it is used as acceptable terminology by AGMA, an attempt will be made to derive the modified Lewis equation for the Novikov system.

The tooth profile is treated as a simple cantilever beam and the weakest section is assumed to be the point of tangency between the inscribed constant stress parabola and the profile. While it is immediately evident that this is not a valid approach, the complexities of a rigorous solution are so great as to discourage any attempt at a solution. Were it possible to find a theoretical solution for even the simplified system we study here (two dimensional with uniform pressure), it would still not apply to the actual gears

Reproduced with permission of the copyright owner. Further reproduction prohibited without permission.

as are used in industry. It is therefore reasonable to use the Lewis factor and let the stress concentration factor as defined from it contain as well the inaccuracies associated with the Lewis factor.

It is possible to derive the Lewis form factor for the Novikov system with relative ease because of the concise geometric relationship between the parameters.

The layout of the convex profile can be seen in figure 2.

obviously: $\beta = S_1/2R_1$

where: R_1 is the radius of the pitch circle

S_1 is the tooth thickness measured along the pitch circle

Also, $\sin\left(\frac{\beta + \varphi_1}{2}\right) = l_1/2R_1$

therefore $\varphi_1 = 2\sin^{-1}\left(\frac{l_1}{2R_1}\right) - \beta$

or $\varphi_1 = 2\tan^{-1}\left(\frac{l_1}{\sqrt{4R_1^2 - l_1^2}}\right) - \beta$

where l_1 is the profile radius drawn from the center P.

The equation of the pitch circle relative to the coordinate system shown in figure 2 is :

$$x^2 + (y - R_1)^2 = R_1^2$$

or $$x^2 + y^2 - 2R_1y = 0 \qquad - ①$$

also $$\sin\left(\frac{\varphi_1}{2}\right) = \sqrt{\frac{x_p^2 + y_p^2}{2R_1}}$$

but from ①

$$x_p^2 = 2R_1y_p - y_p^2 \quad \text{(P is on pitch circle)}$$

therefore $$\sin\left(\frac{\varphi_1}{2}\right) = \sqrt{\frac{y_p}{2R_1}}$$

Reproduced with permission of the copyright owner. Further reproduction prohibited without permission.

then $y_p = 2R_1 \sin^2 (\frac{\varphi_i}{2})$

returning to equation (1)

$$x_p = 2R_1 \sin (\frac{\varphi_i}{2}) \sqrt{1 - \sin^2 (\frac{\varphi_i}{2})}$$

Now to obtain the coordinates of point Q which is the centre of the fillet radius, the use of lemma I (see appendix C) which gives the points of intersection of two circles is necessary .

Substituting :

$a_1 = x_p$ $\quad a_2 = 0$ $\quad r_1 = l_1 + h_1$

$b_1 = y_p$ $\quad b_2 = R_1$ $\quad r_2 = R_1$

where h_1 is the fillet radius

Then from lemma I :

$$A = -2x_p$$

$$B = 2 (R_1 - y_p)$$

$$C = (l_1 + h_1)^2 - x_p^2 - y_p^2$$

by substituting the above values into lemma I it is possible to solve for x_q as the smallest root of a quadratic equation in x_q . Then y_q is determined as

$$y_q = \frac{(l_1 + h_1)^2 - x_p^2 - y_p^2 + 2x_p x_q}{2(R_1 - y_p)}$$

The vertex of the Lewis parabola is defined by :

$$a_n = l_1 \sin (\alpha_d + \varphi_i) - y_p$$

where α_d is the pressure angle

now if the axes are transformed such that

$$x' = x$$

$$y' = y + a_n$$

Reproduced with permission of the copyright owner. Further reproduction prohibited without permission.

then the vertex of the inscribed parabola will be at the origin of the new coordinate system . Now by using lemma II (see appendix C) solve for X and Y the coordinates of the point of tangential intersection between the circle and parabola .

where : $a = x_q$

$b = y_q + a_n$

$r = h_1$

therefore

$$y^4 + (x_q^2 - 2(y_q + a_n)^2 + 2h_1^2)\, y^2 - x_q^2(y_q + a_n)\, y + (x_q^2 + (y_q + a_n)^2 - h_1^2)((y_q + a_n)^2 - h_1^2) = 0$$

This fourth order equation must be solved for Y and this is accomplished by employing the bisection technique . From a consideration of the problem it is evident that there will be two real roots to this equation . One of these will be between $y_q + a_n$ and $y_q + a_n + h_1$; and the other will be between $y_q + a_n$ and $y_q + a_n - h_1$. By studying the geometry of the problem it is possible to choose the root between $y_q + a_n$ and $y_q + a_n + h_1$. Then the solution is carried to the desired degree of accuracy by the bisection technique. Next calculate X as

$$X = \frac{x_q^2 + (y_q + a_n)^2 - h_1^2 - Y^2}{x_q}$$

This gives all the information required to define the Lewis parabola, in that the height is $H = Y$, and the base is $T = 2X$. The Lewis form factor is given as

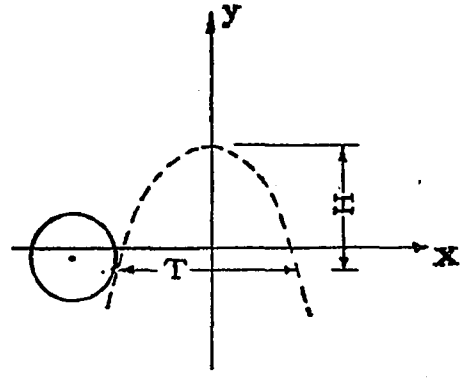

$$Y_n = \frac{T^2}{6H}$$

The layout of the concave tooth is shown in figure 3 . It can be seen that

Reproduced with permission of the copyright owner. Further reproduction prohibited without permission.

$$\beta = 2 \sin^{-1}\left(\frac{l_2}{2R_2}\right)$$

$$= 2 \tan^{-1}\left(\frac{l_2}{4R_2^2 - l_2^2}\right)$$

where l_2 is the concave tooth profile radius

R_2 is the gear radius

also $$\phi = \beta - \frac{S_1 + D}{2R_2}$$

where D is determined from

$$N(S_1 + S_2 + D) = 2\pi R_1$$

or $$D = \frac{\pi}{P} - S_1 - S_2 \qquad \text{since } P = \frac{N}{2R_1}$$

where D is the tooth clearance

but it is also evident from the figure that

$$\phi = 2 \sin^{-1}\left(\frac{\overline{PC}}{2R_2}\right)$$

therefore $$\overline{PC} = 2R_2 \sin\left(\frac{\beta}{2} - \frac{S_1 + D}{4R_2}\right)$$

now $$\gamma_2 = \frac{S_1 + S_2 + D}{2R_2} + 2 \sin^{-1}\left(\frac{\overline{PC}}{2R_2}\right)$$

therefore $$\gamma_2 = \beta + \frac{S_2}{2R_2}$$

where S_2 is the thickness of the concave profile along the pitch circle

The coordinates of the pitch point P are given by

$$y_p = l_2 \sin(2\alpha_d - \delta - \gamma_2)$$

$$x_p = R_2 \sin(\gamma_2)$$

where δ is the cutter clearance angle

Reproduced with permission of the copyright owner. Further reproduction prohibited without permission.

To find the coordinates of point Q the centre of the fillet circle it is necessary to solve for the intersection of the line through PQ and the line through O_2C .

first : the line through P with slope $\tan(2\alpha_\delta - \delta - \varphi_2)$ is

$$x\left(\tan(2\alpha_\delta - \delta - \varphi_2)\right) - y = R_2 \sin(\varphi_2)\tan(2\alpha_\delta - \delta - \varphi_2) - l_2 \sin(2\alpha_\delta - \delta - \varphi_2)$$

second : line through O_2 with slope $1/\tan(\varphi_2 - \phi)$ is

$$\frac{x}{\tan(\varphi_2 - \phi)} - y = R_2 \cos(\varphi_2) - l_2 \sin(2\alpha_\delta - \delta - \varphi_2)$$

solving :

$$x_q = \frac{R_2 \sin(\varphi_2)\tan(2\alpha_\delta - \delta - \varphi_2) - R_2 \cos(\varphi_2)}{\tan(2\alpha_\delta - \delta - \varphi_2) - 1/\tan(\varphi_2 - \phi)}$$

and $$y_q = \frac{x_q}{\tan(\varphi_2 - \phi)} - R_2 \cos(\varphi_2) + l_2 \sin(2\alpha_\delta - \delta - \varphi_2)$$

To find the fillet radius h use the coordinates of the point $M\,(R_2 \sin(\varphi_2) - l_2 \cos(2\alpha_\delta - \delta - \varphi_2), 0)$

now $h = \overline{QM}$

$$\therefore \quad h = \sqrt{(x_q - x_m)^2 + y_q^2}$$

The location of the vertex of the inscribed parabola is given by

$$p_n = y_p - l_2 \sin(\alpha_\delta - \varphi_2)$$

now if the axes are transformed such that

$$x' = x$$
$$y' = y + p_n$$

then the vertex of the parabola will be at the origin .

Reproduced with permission of the copyright owner. Further reproduction prohibited without permission.

It is possible for the parabola to be tangent to two circles at this point, one of which is the fillet and the other is the profile . It is obvious that there will always be a solution with the profile circle, therefore this will be solved for first . Using lemma II

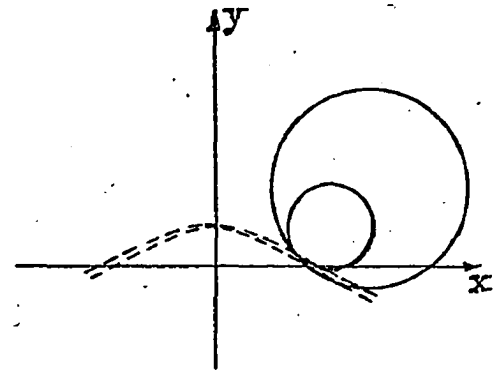

$$a = x_q$$

$$b = y_p - p_n$$

$$r = l_2$$

then substituting

$$y^4 + (x_p^2 - 2(y_p - p_n)^2 + 2l_2^2)\, y^2 - 2x_p^2(y_p - p_n)\, y + (x_p^2 + (y_p - p_n)^2 - l_2^2)((y_p - p_n)^2 - l_2^2) = 0$$

This equation is solved for Y by the bisection technique with the solution lying between $y_p - p_n$ and $y_p - p_n - l_2$. Now if this intersection is the one of interest , it must occur above the x axis

$$\text{i.e.} \quad Y + p_n \geqslant 0$$

if this is so ; then

$$X = \frac{x_p^2 + (y_p - p_n)^2 - l_2^2 - Y^2}{x_p}$$

however if $Y + p_n < 0$ then it is necessary to solve for the intersection with the fillet circle . Again using lemma II

$$a = x_q$$

$$b = y_q - p_n$$

$$r = h$$

then the equation to be solved becomes

Reproduced with permission of the copyright owner. Further reproduction prohibited without permission.

$$y^4 + (x_q^2 - 2(y_q - p_n)^2 + 2h^2)\, y^2 - 2x_q^2(y_q - p_n)\, y$$

$$+ (x_q^2 + (y_q - p_n)^2 - h^2)((y_q - p_n) - h^2) = 0$$

for Y by the bisection technique where the solution lies between $y_q - p_n$ and $y_q - p_n - h$. Also

$$X = \frac{x_q^2 + (y_q - p_n)^2 - h^2 - Y^2}{x_q}$$

This gives the information necessary to define the Lewis parabola

i.e. $H = Y$

$T = 2X$

then the Lewis factor is

$$Y_n = \frac{T^2}{6H}$$

The fact that the load is applied as an area contact rather than a point contact leads to a further assumption . Which is to say that the distributed load p lb/in will be replaced by a point load W_n where

$$W_n = pl_1(2\alpha_s - 2\,\delta)$$

Now this load W_n is not applied at the pitch circle as in the involute system, rather it is applied at $R_1 + a_n$ in the convex tooth and at $R_2 \cos(\varphi_2) - y_p + p_n$ in the concave tooth . Therefore it is convenient to define a pitch circle correction factor :

$$p^*_{convex} = (R_1 + a_n)/R_1$$

$$p^*_{concave} = (R_2 \cos(\varphi_2) + p_n - y_p)/R_2$$

Also, the relation between the load W_n and the transmitted load W_t is defined as

$$W_t = fW_n$$

where: $f_{convex} = \cos(\alpha_s + \varphi_1)$

Reproduced with permission of the copyright owner. Further reproduction prohibited without permission.

$$f_{concave} = \cos(\alpha_f - \rho_2)$$

Then the stress σ is given by

$$\sigma = K_{2-D} \frac{W_t P}{F Y_n}$$

where: W_t = transmitted load (lb)
P = diametral pitch (1/in)
F = tooth length (in)
Y_n = Lewis factor
K_{2-D} = two dimensional stress concentration factor

The values of Y_n, f and p^* were calculated for the values of tooth geometry employed in the experiment.

The values of f and p^* are used in design to determine the relation between the transmitted load W_t and the contact pressure p.

For the gears tested the design variables have the following values :

α_f = 23.2°
f = 7.3°
P_n = 5.44
S_1 = .410 inches
S_2 = .208 inches
D = .008 inches
$\frac{S_1}{S_2} \simeq 2$
$\frac{D}{S_2}$ = .037
$\frac{l_1}{S_1}$ = .999
h = .132 inches
$\frac{h}{l_1}$ = .324

Reproduced with permission of the copyright owner. Further reproduction prohibited without permission.

These values are used in calculating the Lewis factors and related variables shown in figures (4, 5, and 6).

3.2.2 Stress Concentration Factor

Stress concentration factor can be defined as the ratio of the stress actually present at a point in a body to some arbitrarily defined stress. The arbitrary stress is usually based on the applied load and a simple geometric property of the body in question. In the case of gear teeth, it has been common practice to base the stress concentration factor on the Lewis factor. This has been considered a disadvantage because of the difficulty involved in either plotting the Lewis parabola on a large scale drawing of the profile or the use of digital calculation. However, the Novikov system lends itself more readily to this procedure, even though it is necessary to approximate the tooth loading conditions.

The stress concentration factor K_t is defined as

$$K_t = \frac{\sigma_a}{\frac{W_t P}{F Y_n}}$$

Where σ_a = actual stress (maximum) at tooth fillet

W_t = transmitted load (perpendicular to tooth centre line)

P = diametral pitch

F = tooth length

Y_n = Lewis factor

However, in the three dimensional case of gear loading, it appears advantageous to define another factor ψ_σ, which is defined as the ratio of the maximum stress (σ_{max}) along the tooth length to the average value ($\bar{\sigma}$) of the stress.

$$\psi_\sigma = \frac{\sigma_{max}}{\bar{\sigma}}$$

where we define $\bar{\sigma}$ as

$$\bar{\sigma} = \frac{1}{F}\int_{-1}^{+1} \sigma \, d\chi$$

Reproduced with permission of the copyright owner. Further reproduction prohibited without permission.

where σ = actual stress distribution

χ = length variable

Now we define the three dimensional stress concentration factor K_{3-D} as

$$K_{3-D} = \frac{\bar{\sigma}}{\frac{W_t P}{FY_n}}$$

and then

$$\sigma_{max} = K_{3-D} \gamma_{\sigma} \frac{FY_n}{W_t P}$$

3.3 Relation of Loading Point to Angle of Rotation

In the Novikov gearing system, the contact between a pair of teeth is limited to a small area of the teeth and this area of contact moves across the face of the tooth. This type of action is in direct contrast with the line of contact movement in the involute system. A comparison of the involute spur, involute helical and Novikov systems can be seen in Figure 1. The circular arc tooth profiles are not conjugate and therefore uniform transmission of rotation must be acheived by helical action. That is to say that a spur form of this gearing system does not trasmit uniform motion, and in the helical form an axial overlap ratio of more than one must be maintained to achieve uniform motion transmission.

It is necessary to relate the movement of the load point along the tooth to the angular position of the gears. The tooth length (χ) is measured along the axis of the tooth and is defined as +1 at the front end and -1 at the back end (the front end being the one on which the photostress material is placed). The angular position variable (Ψ) is fixed at 0 for contact at the centre of the tooth length (χ =0) and varies from +4 for contact at the front end to -4 for contact at the back end of the gears. However, because the gears are helical and χ is measured from the front end on both the tension and compression sides of the tooth, there is an offset in

Reproduced with permission of the copyright owner. Further reproduction prohibited without permission.

load position. That is to say; for a load position of 0 on the tension sides of the pinion and wheel (these two surfaces being in contact), the projected load position on the pinion compression side is shifted to a positive value of χ, while on the wheel compression side, it is shifted to a negative value of χ. This effect is illustrated in figure 7 where the load position and projected load positions are plotted against γ.

The angle of rotation involved to vary γ from +4 to -4 is 26.7 degrees for the pinion and 13.6 degrees for the wheel. Because overlap of contact between teeth is necessary and will affect the load carried by the tooth being studied, it is necessary to know when we have multiple contact. Single tooth contact is in effect only for $2 \geqslant \gamma \geqslant -2$, while between 2 and 4 and -2 and -4, two teeth are in contact.

3.4 Major Assumptions Involved

The assumptions which may affect the generality of the results are as follows:

1) In the analysis of the photostress information from the surface of the gears, it is assumed that there is essentially a biaxial state of stress present and that there is no bending of the plane on which the photostress is mounted.

2) At the root section of the tooth the bending stress results in a uniaxial state of stress on the free surfaces.

3) It is assumed that the positions of maximum stress, as obtained from the photostress experiment, do not vary along the length of the tooth since strain gages, which are mounted along the length of the tooth (figure 8), are mounted in a geometrically similar position.

4) The centre to centre distance was 4.000 inches and was constant under loading.

5) Shafts were dead parallel and remained so under loading.

6) Tooth deflection is negligible or did not appreciably affect results.

Reproduced with permission of the copyright owner. Further reproduction prohibited without permission.

3.5 Details of Photoelastic Model

The photoelastic tests were carried out in a transmission polariscope using a polyester material called PSM-1 as the model material. The models of the concave and convex profiles were designed to correspond to a normal section of the metal gears tested. Geometrically they are similar, with only the scale being changed. The diametral pitch of the photoelastic model was 1, whereas the metal gears had a diametral pitch of 5.

The convex and concave models were both made with three teeth, one on either side of the tooth being studied. This was done to more closely approximate the actual condition in a gear set.

The dimensions of the two models can be seen in figure 9. This drawing is full scale.

Reproduced with permission of the copyright owner. Further reproduction prohibited without permission.

4. EXPERIMENTAL ARRANGEMENT AND PROCEDURE

4.1 The Photostress Study

The photostress material was placed on the front ends of both the pinion and the wheel for several teeth on either side of the teeth being tested (see figure 10). The material thickness was 1/8 of an inch; this gives a plastic to metal ratio of 0.0625 which makes the reinforcing effect of the plastic negligible (see appendix D). The photostress material was filed to the shape of the tooth after glueing to the surface. The edge of the photostress was kept normal to the end of the tooth to determine the maximum edge stress.

The stress (fringe) values were obtained using a reflection polariscope and telemicroscope arrangement. A green monochromatic filter was used in obtaining the readings, in order to provide better fringe distinction. The fringe patterns can be seen in figures 11 and 12.

The gears were then loaded to a transmitted load of 2,750 lbs. at various relative angles of rotation and the fringe orders read at four positions. These were the maximum values on the pinion and wheel, tension and compression sides. The positions of these maximum values were also noted in order to locate the critical area for mounting the strain gages.

4.2 The Strain Gage Study

Temperature compensated strain gages were located along the length of the teeth at the positions shown in figure 8. They were along the fillet at the critical positions indicated by the photostress study. The axis of the gage was placed in the plane of normal tooth load. The grid size was 1/32 inch square and due to a lack of room at the bottom land of the tooth it was necessary to place the gage tabs at one end face of the gear and run single strands to the foil gages. These single strands were then insulated to prevent any interconnection of the gages. The strain gages were mounted using Eastman 910 high elongation cement. They were then waterproofed to prevent deterioration during the duration of the experiment. The

Reproduced with permission of the copyright owner. Further reproduction prohibited without permission.

gages were connected through a switch and balance unit to a static strain indicator. The mode of operation was a single active arm strain gage bridge employing an internal dummy resistor and a three lead wire system.

Strain readings were taken for various values of relative angle of rotation of the gears for a transmitted load of 2,750 lbs.

4.3 The Photoelastic Study

The photoelastic models were designed to correspond to a normal section through the metal gears, as is outlined in section 3.5. The tests were carried out in a circular polariscope employing monochromatic light. The method in which the gears were loaded is outlined in Appendix B.

In figures 13 and 14 it is possible to see the resultant fringe patterns for two loads. In figure 15 the variation of fringe order versus load is plotted and this information is then used to obtain the stress concentration information.

Reproduced with permission of the copyright owner. Further reproduction prohibited without permission.

5. RESULTS AND DISCUSSION OF THE ANALYSIS

5.1 Photostress Results

The photostress experiment provides values of the stresses on the front end of the tooth and in figures 11 and 12 it is possible to see the fringe patterns which result. From these, it is possible to locate the points of maximum bending stress on the pinion and wheel teeth. It is evident that the maximum stress occurs on the pinion compression side, with the minimum (in magnitude) stress occurring on the wheel tension side. The results for various values of angle of rotation are shown in figures 16 - 19.

Ψ is defined as a non dimensional angular position variable. A change in Ψ from -4 to +4 corresponds to one complete tooth engagement cycle. The tooth engagement cycle consists of a movement of the contact point from one end of the tooth to the other.

Ψ then is the connecting variable between rotation of the wheel and pinion where a change in Ψ of 8 corresponds to rotating the pinion 26.7° and the wheel 13.6°.

The bending stress at the tooth fillets is σ ; however, the stress is nondimensionalized in order to make it more useful. This is done by introducing the ratio $\frac{\sigma F}{W_t P}$

where σ = stress (psi)

F = tooth length (in)

W_t = transmitted load (lb.)

P = diametral pitch

It can be easily shown that this ratio is related to the Lewis factor.

These graphs are plots of the maximum bending stresses for the four points mentioned. These four points correspond to the points of maximum bending stress on the pinion and wheel teeth fillets.

In figure 16 for the maximum pinion tension stress variation, it is shown that the tooth picks up the load very quickly as engagement begins at $\Psi = -5$ until at $\Psi = -3\frac{1}{2}$ this stress is a maximum. This motion corresponds to an angle of rotation of $3\frac{1}{2}^\circ$.

Reproduced with permission of the copyright owner. Further reproduction prohibited without permission.

After the maximum stress is reached at $\Psi = -3\frac{1}{2}$, the stress decreases steadily until $\Psi = -\frac{1}{2}$ after which the stress is essentially zero. This indicates that the portion of the tooth near the front end is stressed only for about $\frac{1}{2}$ of the period of tooth engagement.

In figure 17 for the maximum pinion compression stress variation angle of rotation required to accept full load=$1\frac{1}{2}^{\circ}$. The maximum stress is reached at $\Psi = -3\frac{1}{2}$; however the stress does not return to zero for the range of tooth loading shown. This indicates that the front face of the tooth in this area is stressed throughout the period of tooth engagement. This must be due to the fact that the adjacent tooth (on the pinion compression side) bending stresses are such that they produce stresses at the locations being studied.

In figure 18 for the maximum wheel tension stress variation, the angle of rotation required to accept the full load is 1.7° of wheel rotation. After the maximum stress is reached at $\Psi = -3\frac{1}{2}$ the stress gradually decreases to essentially zero at $\Psi=0$. This again indicates that the front portion of the tooth is stressed only for about $\frac{1}{2}$ of the period of tooth engagement.

In figure 19 for the maximum wheel compression stress variation, the angle of rotation required for acceptance of the full load is 1°. The maximum value of the bending stress is reached for $\Psi = -3\frac{1}{2}$. However, after this point, the stress does not return to zero and remain zero but instead steadily decreases to a tensile stress which has a maximum value near $\Psi = 2$, after which it drops towards zero again.

All four positions studied show a maximum value of bending stress at $\Psi = -3\frac{1}{2}$. The values of the bending stress, $\frac{\sigma F}{W_t P}$ at this value of Ψ are:

Pinion	tension	1.7
	compression	-3.0
Wheel	tension	+1.3
	compression	-1.4

The positions of the four maximum stresses do not change with the angular position variable Ψ. In all cases the load is picked up very quickly. This could lead to large dynamic effects

Reproduced with permission of the copyright owner. Further reproduction prohibited without permission.

when the gears are transmitting motion as well as load. The position at which the maximum stress occurs is dependent upon two factors. One of these is the fact that the tooth is more flexible near the end and therefore accepts the load gradually. At the same time the load is moving along the tooth length as γ increases. These two effects balance such that the maximum stresses occur at $\gamma = -3\frac{1}{2}$ as was indicated.

5.2 Strain Gage Results

The strain gage results extend the photostress experiment to include the fact that the loading is short compared to the overall tooth length. The location of the strain gages can be seen in figure 8.

In figure 20 the stress variation with angle of rotation for each of the positions tested on the pinion tension side is shown. The stress at each of these positions rises to a maximum and then drops off again. It is evident that there is symmetry of the maxima about $\gamma = 0$ for gages 1 and 5, 2 and 4, and gage 3. This symmetry is to be expected, but it is not perfect symmetry since the gages are not mounted exactly symmetrically about the center line of the tooth length. The maximum stress occurs for central loading at the central gage position. For $\gamma > 4$ the instrumented tooth is no longer being loaded and the compressive stresses which became evident for $\gamma \simeq 6$ is due to stressing of the next tooth on the pinion. The maximum stress variation $(\frac{\sigma F}{W_t P})$ during rotation encountered is +5.72 to -1.20 for the center gage.

In figure 21 the variation of stress with angle of rotation is shown on the pinion compression side for the positions tested. Again the stress rises to a maximum (compressive) and falls off to zero. That the maximum does not occur at $\gamma \simeq 0$ is explained in figure 7. The maximum stress variation $(\frac{\sigma F}{W_t P})$ is -7.80 to +1.80 for gage 4.

In figure 22 the maximum stress variation with angle of rotation is shown for the wheel tension side. These curves are similar to the curves for the pinion tension side with the only significant difference being magnitude. The maximum stress variation is 6.20 to - 1.70 for the center gage.

Reproduced with permission of the copyright owner. Further reproduction prohibited without permission.

In figure 23 the maximum stress variation with angle of rotation is shown for the wheel compression positions tested. These curves are similar to those for the pinion compression except that the magnitudes of the stresses are different and in this case tensile stresses occur for values of $\Psi > 0$. The maximum stress variation is -8.50 to +2.50 for the center position.

In figures 24-27 the information is plotted to show the stress variation along the length of the tooth for sixteen different loading positions. The values of Ψ between -2 and +2 represent single tooth contact; values of Ψ between -2 and -4 and +2 and +4 represent double tooth contact. Both the maximum value of stress and shape of these curves changes with Ψ.

In figure 24, for the pinion tension stresses, the maximum value of $\frac{\sigma F}{W_t P}$ occurs for $\Psi = \frac{1}{2}$. The maximum values for the pinion compression and wheel compression stress also occur at $\frac{1}{2}$. However, the maximum value for the wheel tension stress occurs for $\Psi = 0$. It is, however, difficult to say if the curves shown are very accurate since only five points are available on each curve and the stress gradients are extremely high. The presence of high stress gradients also puts the accuracy of the strain gage readings into doubt since they indicate the average stress over the gage width. It can be seen in figure 24, for the pinion tension side, that for Ψ between $-1\frac{1}{2}$ and $1\frac{1}{2}$ (where there is single tooth contact) that there is very little variation in the maximum value of $\frac{\sigma F}{W_t P}$. However for Ψ outside this range, the stress is considerably lower which is due to double tooth contact. The same type of trend is maintained for the other 3 points tested as can be seen in figures 25, 26 and 27.

Figures 28, 29, 30 compare the stresses at the four points studied for three values of Ψ ($-\frac{1}{2}, \frac{1}{2}, 0$). As can be seen, the tension values (wheel and pinion) have their maximum at approximately the same value of X. This value of X corresponds to that predicted for the load position as determined from Ψ (see figure 7). The wheel maximum tensile stress is also greater than the pinion maximum tensile stress. The compression values, however, are shifted (again corresponding to figure 7) from the value of X at which the load is applied.

Reproduced with permission of the copyright owner. Further reproduction prohibited without permission.

In figure 30 the stress values predicted by Wellauer and Seireg (reference 11) are also plotted. These stresses from Wellauer and Seireg are less than those recorded.

5.3 Photoelastic Results

In figures 13 and 14 the isochromatic fringe patterns resulting in the tooth profiles for normal loads of 27.9 and 34.9 pounds are shown. From these photographs the positions of the maximum tensile and compressive stresses in the wheel and pinion are evident. It can be seen that adjacent teeth are not stressed by the loading. This is not in agreement with the actual gear tests and shows one of the shortcomings of the two dimensional tests. The variation of fringe order with load can be seen in figure 15. From the slopes of these curves and the calibration of the material, it is possible to obtain the stress concentration factors.

5.4 Combined Analysis

The strain gage results have been extrapolated to the end of the tooth as shown in figures 24, 25, 26 and 27 and these values may be compared to the photostress results which are obtained only at the end of the tooth. The results are compared in figures 16, 17, 18 and 19. The maximum values of the extrapolated strain gage results are in all cases greater than the photostress results in the range of 10% to 37%. For the stress equal to zero, the two curves cross. This would seem to indicate that the interpretation of the fringe order information is in question. However, both sets of results, obtained by two different methods, show the same variation of stress, even though they differ in magnitude. This indicates that the photostress technique will predict the relative magnitude of the stresses; however the actual value is not obtained by this method. The pinion results compare more closely than the wheel results. A possible explanation of this is the greater flexibility of the wheel teeth (which are thinner) which then does not distribute the stress as well over the tooth length as the stiffer pinion tooth does. In order to choose the proper photostress correction factor, it is necessary to know how much of the tooth is supporting the load. Since this is not known the photostress results become qualitative

Reproduced with permission of the copyright owner. Further reproduction prohibited without permission.

rather than quantitative.

Figures 11, 12, 13 and 14, which show the isochromatic fringe patterns for the photostress and photoelastic tests indicate similar patterns. The locations of the maximum bending stresses are similar for both cases. This indicates that the photostress technique does allow the determination of the location of the maximum bending stresses in the gear teeth.

In order to compare the results of the two dimensional photoelastic model tests and the three dimensional strain gage study, it is necessary to define the following stress concentration factors:

$$K_{2-D} = \frac{\sigma F Y_n}{W_t P}$$

and $$K_{3-D} = \frac{\bar{\sigma} F Y_n}{W_t P}$$

where $$\bar{\sigma} = \frac{1}{F}\int_{-1}^{+1} \sigma \, d\chi$$

The values of $\bar{\sigma}$ are shown in figure 31. These values are obtained by integrating the curves obtained for the stress variation from the strain gage results (figures 24-27). The values remain relatively constant in the range $-2<\psi<2$ which is the limitation on single tooth action. The results predicted by Wellauer and Seireg (11), (which only predict the compressive stresses) are also plotted; their theoretical analysis predicts a constant value of $\bar{\sigma}$. The tension bending stresses most closely follow the prediction of a constant value. These results would indicate then that $\bar{\sigma}$ = a constant, is at least a reasonable approximation to the variation in $\bar{\sigma}$ (for single tooth contact). It is for this reason that the three dimensional stress concentration factor is based on $\bar{\sigma}$. That is to say K_{3-D} becomes independent of the point of tooth loading. It does require, however, that a new variable be introduced. This variable is ψ_σ and it is defined as a stress distribution factor:

$$\psi_\sigma = \frac{\sigma_{max}}{\bar{\sigma}}$$

Reproduced with permission of the copyright owner. Further reproduction prohibited without permission.

where σ_{max} = maximum stress along tooth profile.

The variation of ψ_σ with angle of rotation is plotted in figure 32 and it is essentially constant for $-2<\gamma<2$ (the range of single tooth contact). Wellauer and Seireg also predict a constant value in this range and their results are also shown in this figure. The fact that there is multiple tooth contact outside this range causes the values of ψ_σ to decrease while the theory predicts an increase. Thus in a system with a reasonable overlap ratio (in this case equal to 1.25), the largest value of ψ_σ will be encountered for central loading.

The stress concentration factors are compared in figure 33. The comparison between the two dimensional and three dimensional results is very good, with the maximum difference between the two sets of results being 14% for the pinion compression stresses. This indicates that it is possible to extend the results of a simpler two dimensional study into the three dimensional case to predict the value of $\bar{\sigma}$. Comparison with the values of K, predicted by Wellauer and Seireg (11), is good for the pinion (10% difference), but poor for the wheel (28% difference). The values given by Fedyakin and Chesnokov (5) agree closely with the experimental values (8% difference); however, only compression values are available. While the compressive stresses are a maximum due to the combined effects of bending and direct load on the tooth, these stresses do not have any important role in the fatigue failure of the tooth since this phenomenon is due primarily to tensile stresses; hence the importance of the tensile stresses.

The values of ψ_σ are compared in figure 34. The values shown are for $\gamma = 0$. The values are not in agreement which may be expected since they are based on different systems.

Application of the results of Wellauer and Seireg to this study is useful in that their results predict the trends which occur. However, the magnitudes of K_t, ψ_σ and $\bar{\sigma}$ which they present are incorrect in magnitude. This is partially due to the fact that they do not consider tooth flexibility in their derivation. The ratio of tooth length to height is also neglected in determining the stress

248700

Reproduced with permission of the copyright owner. Further reproduction prohibited without permission.

distribution.

The results obtained for the stress concentration factor may be employed to compare the studied gear system to a comparative involute system. The values for the involute system will be taken from Shigley (18).

$$\sigma = \frac{W_t P}{F Y_n} K \psi_\sigma$$

where W_t, P and F will be set the same for both systems, also the helix angle and pressure angle will be fixed

$$\text{then } \frac{\sigma F}{W_t P} = \frac{K \psi_\sigma}{Y_n}$$

for the spur gear system $\psi_\sigma = 1$ (this is not likely in practice). The tension stresses are those of interest and they give rise to the following results:

	spur involute	helical involute	Novikov
pinion tension	4.30	2.13	4.70
wheel tension	3.70	1.90	5.70

It is obvious that the Novikov profile tested is weaker in bending than the helical involute profile, while the pinion tension bending stress is comparable to the stresses in a similar involute spur gear system.

5.5 Estimate of the Experimental Error

The photostress results depend upon the accuracy with which the fringe orders can be read. Since the fringe count was usually of the order of one fringe and the accuracy of the recordings is $\pm$ 0.1 fringe; this corresponds to an error of approximately $\pm$ 1350 psi in the magnitude of the maximum stress encountered or an error of $\pm$ 7%. Repeatability of readings was well within this tolerance.

The tolerance on the strain gage readings is $\pm$ 10 micro in./in. This accuracy is fixed by the indicator accuracy ($\pm$ 2μ in./in.) and temperature variation in the room ($\pm$ 10 F° maximum during testing period). This error corresponds to a variation of $\pm$ 300 psi in the tooth bending stress. For the maximum stress recorded, this corresponds to a possible error of 0.2%.

Reproduced with permission of the copyright owner. Further reproduction prohibited without permission.

Repeatability of loading at this maximum recorded stress was $\pm$ 100 μ in./in., which corresponds to a tolerance of $\pm$ 2% of the stress value.

The accuracy of the photoelastic study depends upon the determination of the fringe order at the fillet boundary. The determination of the partial fringe order was done by means of Tardy compensation and the readings were repeatable within $\pm$ 5 degrees. For the maximum reading encountered, this is equivalent to a possible error of $\pm$ 1.5%.

The angular position of the gear tooth was measured by means of a long pointer and scale arrangement and this position could be fixed within $\pm$ .5 degrees (of pinion rotation) which corresponds to a possible error in the value of χ of .02 (out of a maximum value of 2); that is $\pm$ 1%.

The load applied to the metal gears was monitored by a strain gage transducer which was temperature compensated. This set up was readable to within $\pm$ 5 μ in./in. The experiment was run at a strain reading of 800 μ in./in., corresponding to a possible error of 0.6%. Repeatability of loading was $\pm$ 25 μ in./in. (arm) for the same value of load at the gear teeth. This corresponds to a possible error of 3% in the value of the load.

Other possible sources of error which are difficult to estimate, but were judged to be small are:

1) location of gages along the tooth length. Since there is a finite gage length (1/32") an average is obtained along a normal section through the tooth. It is also possible that the gage was not centered on the point determined from the photostress study, since the root of the tooth is not readily accessible. However, variations in this distance were not measurable.

2) movement of the gears under load. The loading frame was designed to minimize these effects; however, it is impossible to avoid some deflection of the structure under loading. Changes in the centre to centre distance would result in changes in the stresses encountered. This variation is mentioned by T. Allan (2) in his work with two dimensional profiles.

Reproduced with permission of the copyright owner. Further reproduction prohibited without permission.

3) tooth deflection may be a slight problem since the loads applied here are far greater than those normally encountered in practice.

Reproduced with permission of the copyright owner. Further reproduction prohibited without permission.

6. RECOMMENDATIONS

6.1 Suggestions for Experimental Improvement

It would be desirable to improve the accuracy and sensitivity of the photostress experiment. One possible way of doing this may be to go to a thicker layer of photoelastic material; however, care must be exercised to prevent larger reinforcing effects. The accuracy of the photostress method would be greater if it were possible to determine what portion of the tooth is carrying the load and then apply a correction factor for the reinforcing effect properly.

The strain gage results are satisfactory; however, more accurate determination of the stress variation would be possible if more gages had been used along the length of the tooth. This would improve the determination of $\bar{\sigma}$ and σ_{max}.

6.2 Suggestions for Future Work

1) A three dimensional photoelastic study would provide information on whether the assumption that the photostress (edge information) results predict the position of the maximum stress along the tooth length, is valid.

2) A study of the effect of centre distance variation on a set of test gears.

3) A two dimensional study which would determine the effect of design variables (α_δ, δ, l_1, h, S_1, S_2, D) on the stress concentration factor.

h = fillet radius
α_δ = pressure angle
δ = cutter clearance angle
l_1 = profile radius
S_1 = convex tooth thickness
S_2 = concave tooth thickness
D = tooth clearance

It would also be possible to consider centre to centre distance and the number of teeth.

4) A study of various systems to see which variables affect ψ_σ. The simplest case of this would be a simple cantilever plate in

Reproduced with permission of the copyright owner. Further reproduction prohibited without permission.

which the variables of interest would be the length, width, thickness and load position.

5) A study to see what minimum overlap ratio is necessary in order to maintain γ_T a constant during rotation of the gear system.

6) Dynamic tests involving gear sets operating at various speeds.

7) A study of the contact stresses to determine the influence of design parameters on wear and pitting.

Reproduced with permission of the copyright owner. Further reproduction prohibited without permission.

7. CONCLUSIONS

1) The photostress technique allows a convenient means of determining the location of the maximum bending stresses in helical gear forms (at the edge of the tooth). However, the magnitude of the edge stress readings is influenced by the flexibility of the teeth. Also, the method lacks sensitivity.

2) By defining

$$K_{3-D} = \frac{1}{F}\int_{-1}^{+1} \sigma \, d\chi \, \frac{FY_n}{W_t P}$$

it is possible to obtain good agreement between the two dimensional and three dimensional stress concentration factors. Then by employing the further factor $\psi_\sigma = \frac{\sigma_{max}}{\bar{\sigma}}$ we have:

$$\sigma_{max} = K_{\binom{2-D}{3-D}} \psi_\sigma \frac{W_t P}{FY_n}$$

as the equation predicting the maximum bending stress , where ψ_σ can be determined experimentally by a three dimensional test or by a theoretical estimation .

3) Reasonable agreement is obtained with the results presented by references (11)and (5) and stress concentration factors are presented for the tension side of the profiles tested (see figure 33).

4) For the value of axial overlap tested here (1.25) it was found that the worst condition of loading is central loading and not end loading of the tooth.

5) The locations of the positions of maximum stress from the photoelastic and photostress experiments agree. This would seem to support the assumption that these critical positions are constant along the length of the tooth.

6) The Lewis Factor for the Novikov system of gearing is determined algebraicly without need for an approximate solution. This makes the Lewis Factor a more useful concept for this gear form than it is for the involute system.

7) The Novikov profile tested here is weaker in bending than a comparable involute system (by approximately a factor of 2).

Reproduced with permission of the copyright owner. Further reproduction prohibited without permission.

Thus the advantages claimed for the Novikov system must be due to improved contact stresses and not bending stress.

Reproduced with permission of the copyright owner. Further reproduction prohibited without permission.

8. BIBLIOGRAPHY

1. Klein, G. J., "Wildhaber-Novikov System of Gearing", Canada National Research Council Quarterly Bult., Report DME/NAE(1), 1965, p. 65-98.
2. Allan, T., "Some Aspects of Design and Performance of Wildhaber-Novikov Gearing", Institution of Mechanical Engineers - Proceedings, Volume 179, number 30, 1964-65, p. 931-54.
3. French, M. J., "Gear Conformity and Load Capacity", Institution of Mechanical Engineers - Proceedings, 1965-66, part 1, number 43, p. 1013-24.
4. Fediankan, R. W. and Tschechonow, W. A., "Gear Transmission with the Novikov System", Vestnik Mashin, May, 1958.
5. Fediankan, R. W. and Tschechonow, W. A., "Calculations for the Novikov System", Vestnik Mashin, June, 1958.
6. French, M. J., "Conformity of Circular Arc Gears", Journal of Mechanical Engineering Sciences, volume 7, number 2, June, 1965, p. 220-3.
7. Wildhaber, E., "Helical Gearing", U. S. Patent 1601750, October 5, 1926.
8. Wildhaber, E., "Method of Grinding Gears", U. S. Patent 1858568, May 17, 1932.
9. Thompson, G. B., "The Shape of Gear Teeth", The New Scientist, March, 1960.
10. Wells, C. F. and Shotter, B. A., "The Development of Circarc Gearing", AEI Engineering, Vol. 2., No. 2.
11. Wellauer, E. J. and Seireg, A., "Bending Strength of Gear Teeth by Cantilever Plate Theory", ASME Journal of Engineering for Industry, June, 1960, p. 213-220.
12. Kaluzhnikov, A. N., "A New Point-Contact System for Gear Teeth", Izobretatelstov V SSSR, No. 11, 1957, p. 26-27, 30-31.
13. Davies, W. J., "Novikov Gearing", Machinery, Volume 96, January 13, 1960, p. 64-73.
14. Walker, H., "A Critical Look at the Novikov Gear", The Engineer, April 29, 1960, p. 725-729.

Reproduced with permission of the copyright owner. Further reproduction prohibited without permission.

15. Wells, C. F., "Current Developments in Gear Engineering (AEI)", AEI Engineering, Volume 6, number 6, Nov.-Dec., 1966, p. 306-310.

16. Kugimiya, H., "Stresses in Helical Gear Teeth", Japan Society of Mechanical Engineers, 1966, p. 816.

17. Johnson, D. C., "Gear Teeth with Circular Arc Profiles", Engineering, 1959, p. 294.

18. Shigley, J. E., "Mechanical Engineering Design", Mcgraw Hill, 1963.

Reproduced with permission of the copyright owner. Further reproduction prohibited without permission.

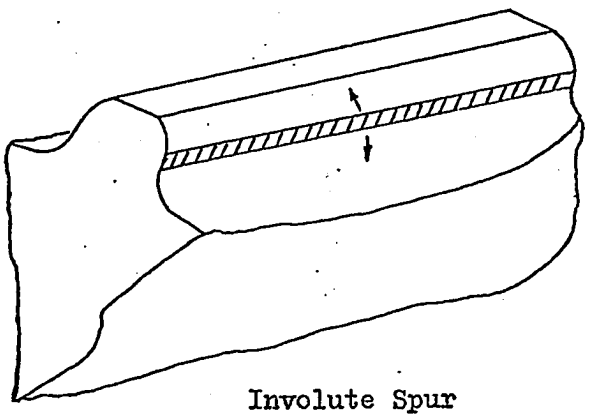

Involute Spur

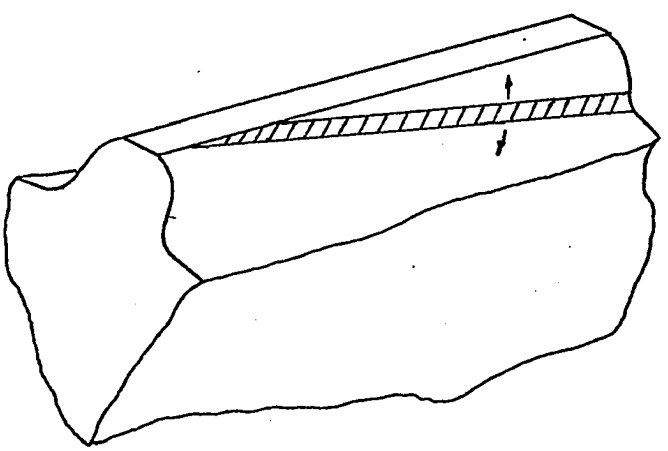

Involute Helical

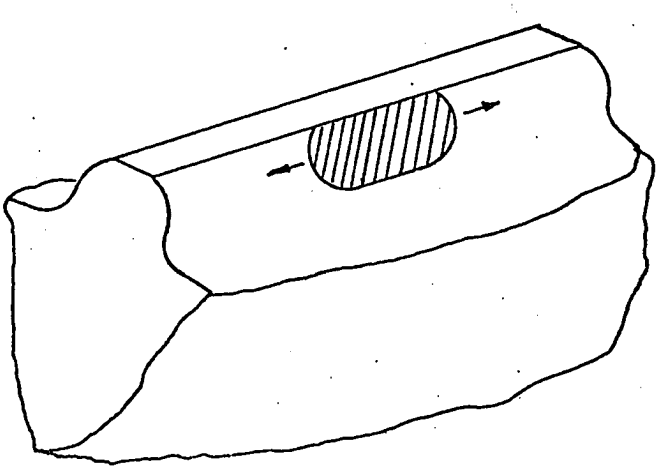

Novikov

Fig. 1 Comparison of Tooth Contact in the Novikov and Involute Systems

Reproduced with permission of the copyright owner. Further reproduction prohibited without permission.

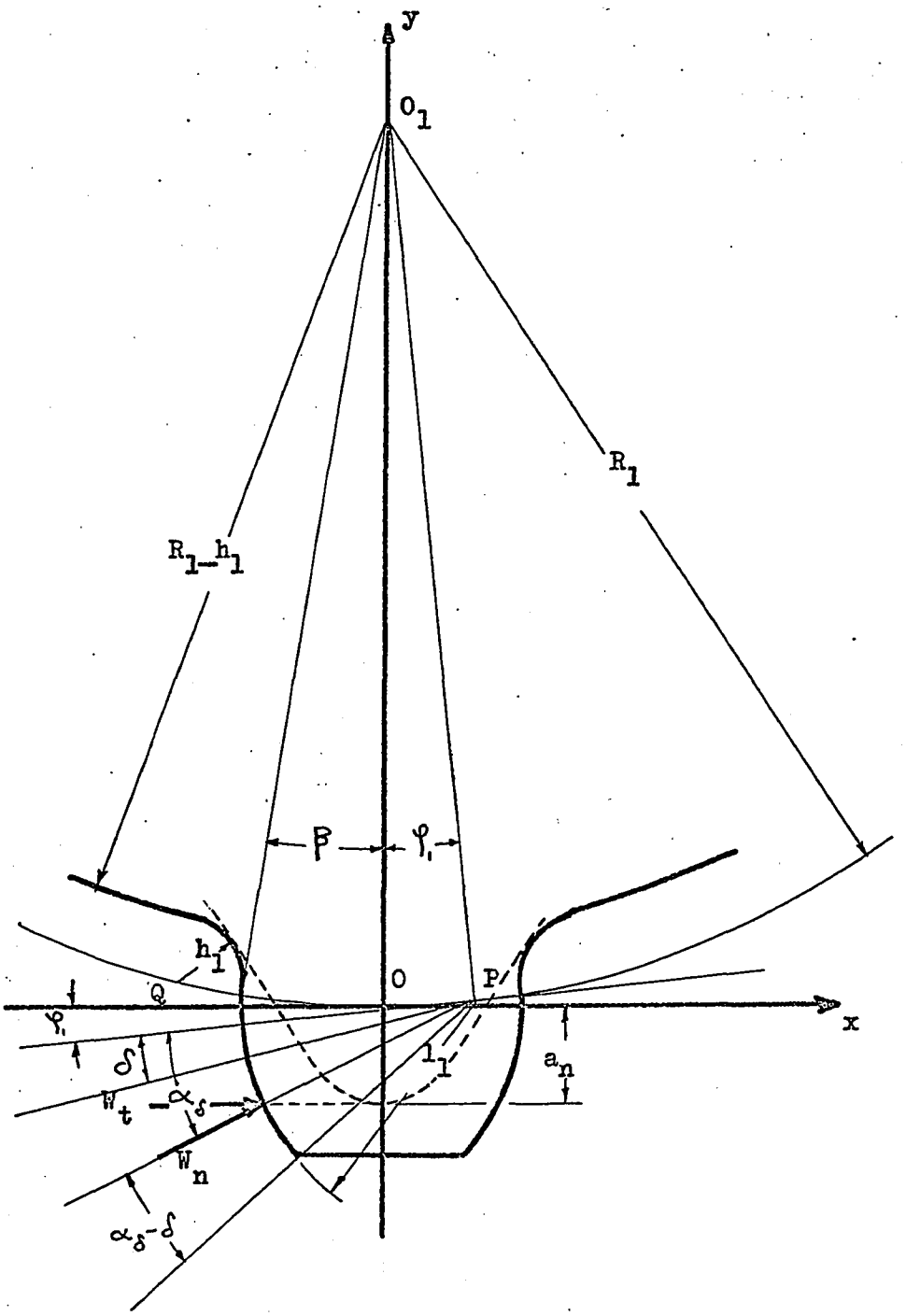

Fig. 2 Convex Tooth Geometry

Reproduced with permission of the copyright owner. Further reproduction prohibited without permission.

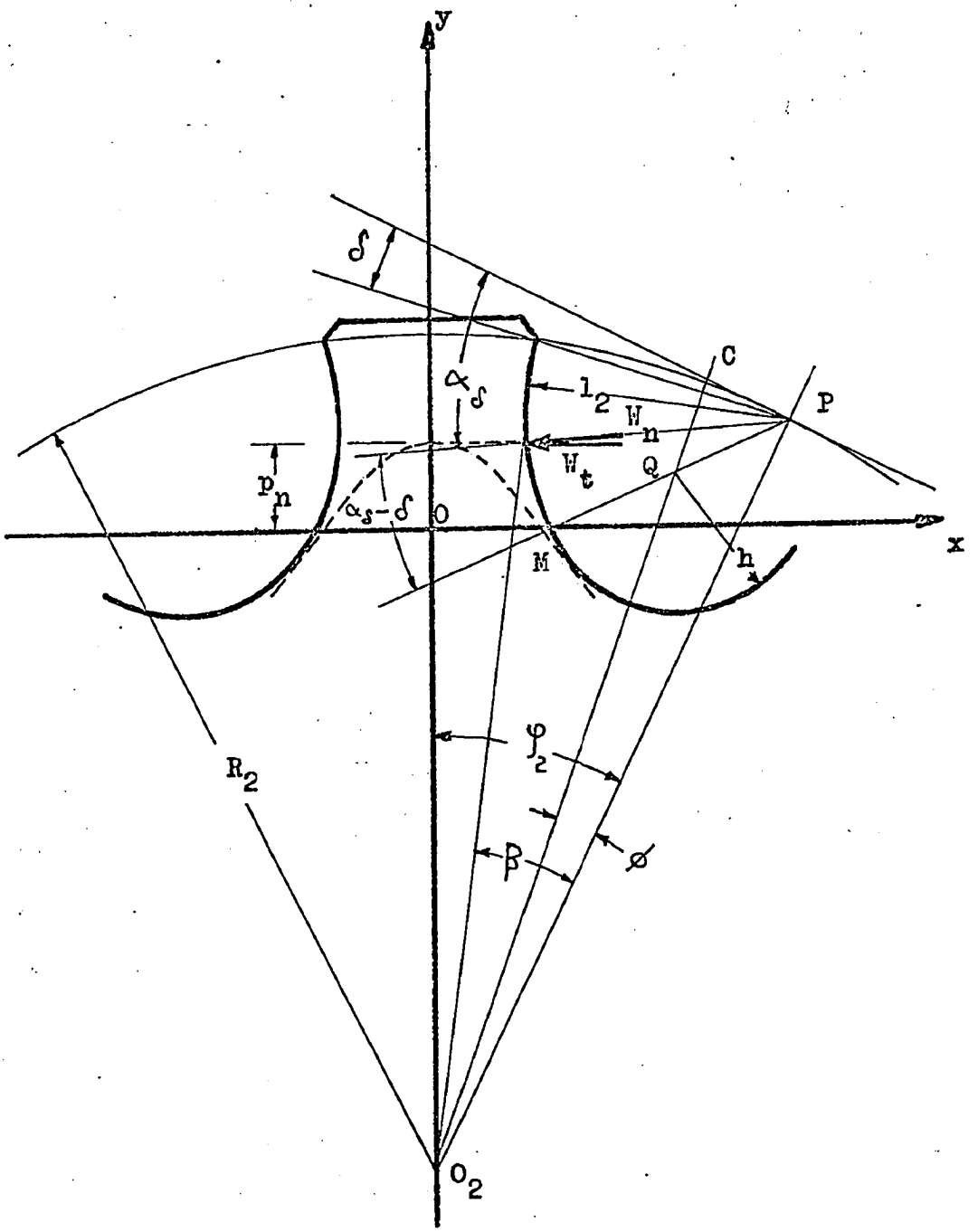

Fig. 3 Concave Tooth Geometry

Reproduced with permission of the copyright owner. Further reproduction prohibited without permission.

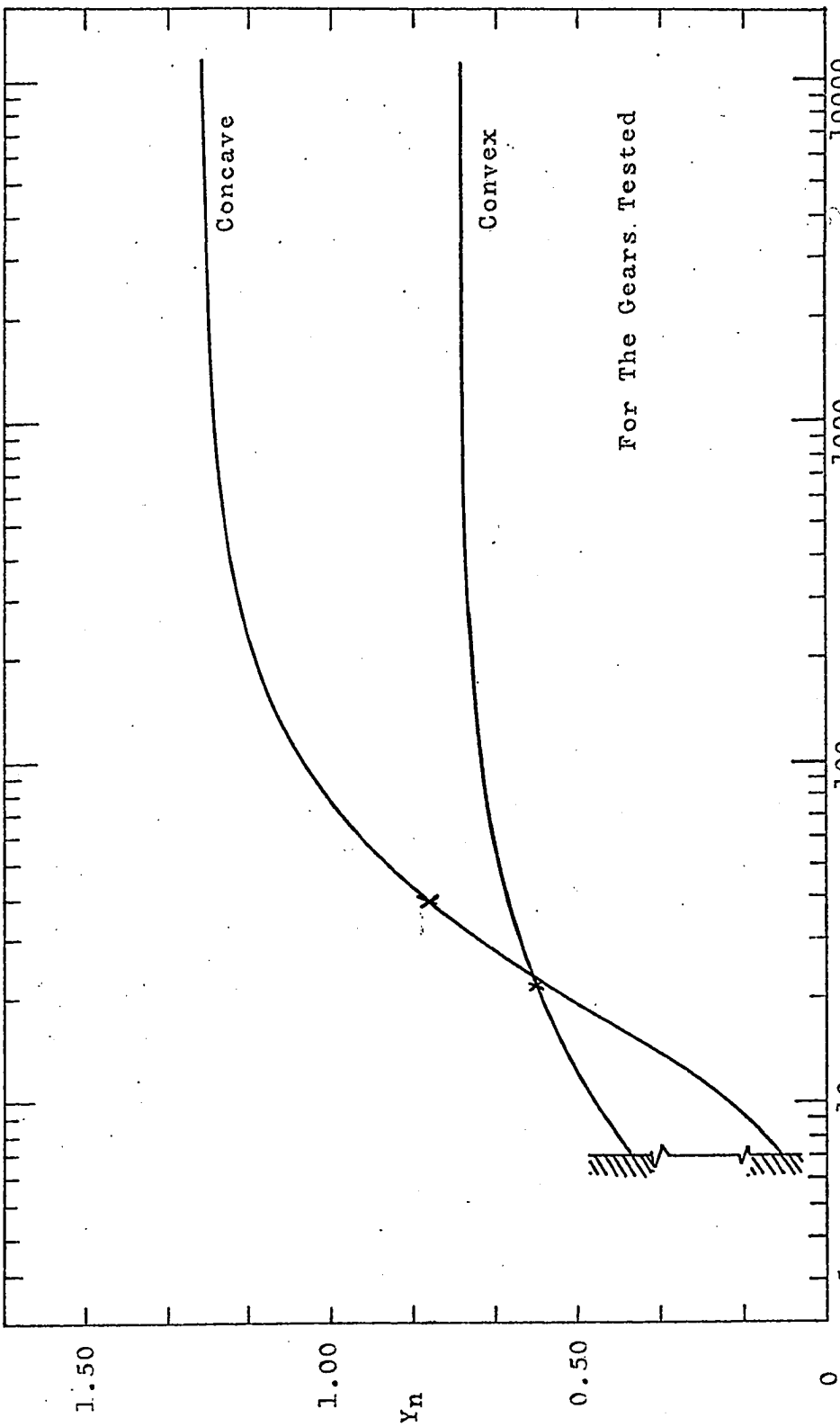

Fig. 4 LEWIS FACTOR Y_n vs Number of Teeth N

Reproduced with permission of the copyright owner. Further reproduction prohibited without permission.

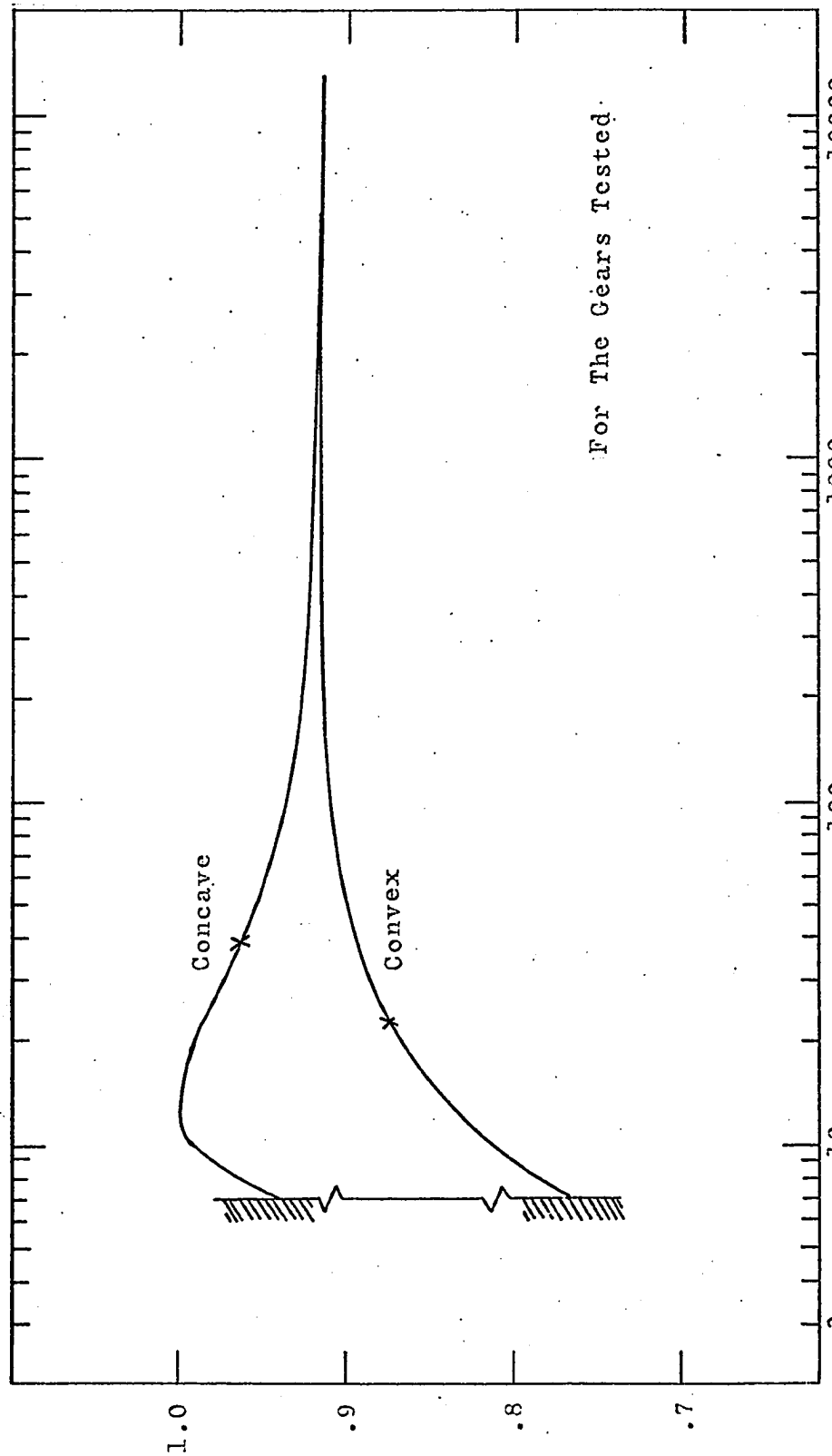

Fig. 5 Load Correction Factor f vs Number of Teeth N

Reproduced with permission of the copyright owner. Further reproduction prohibited without permission.

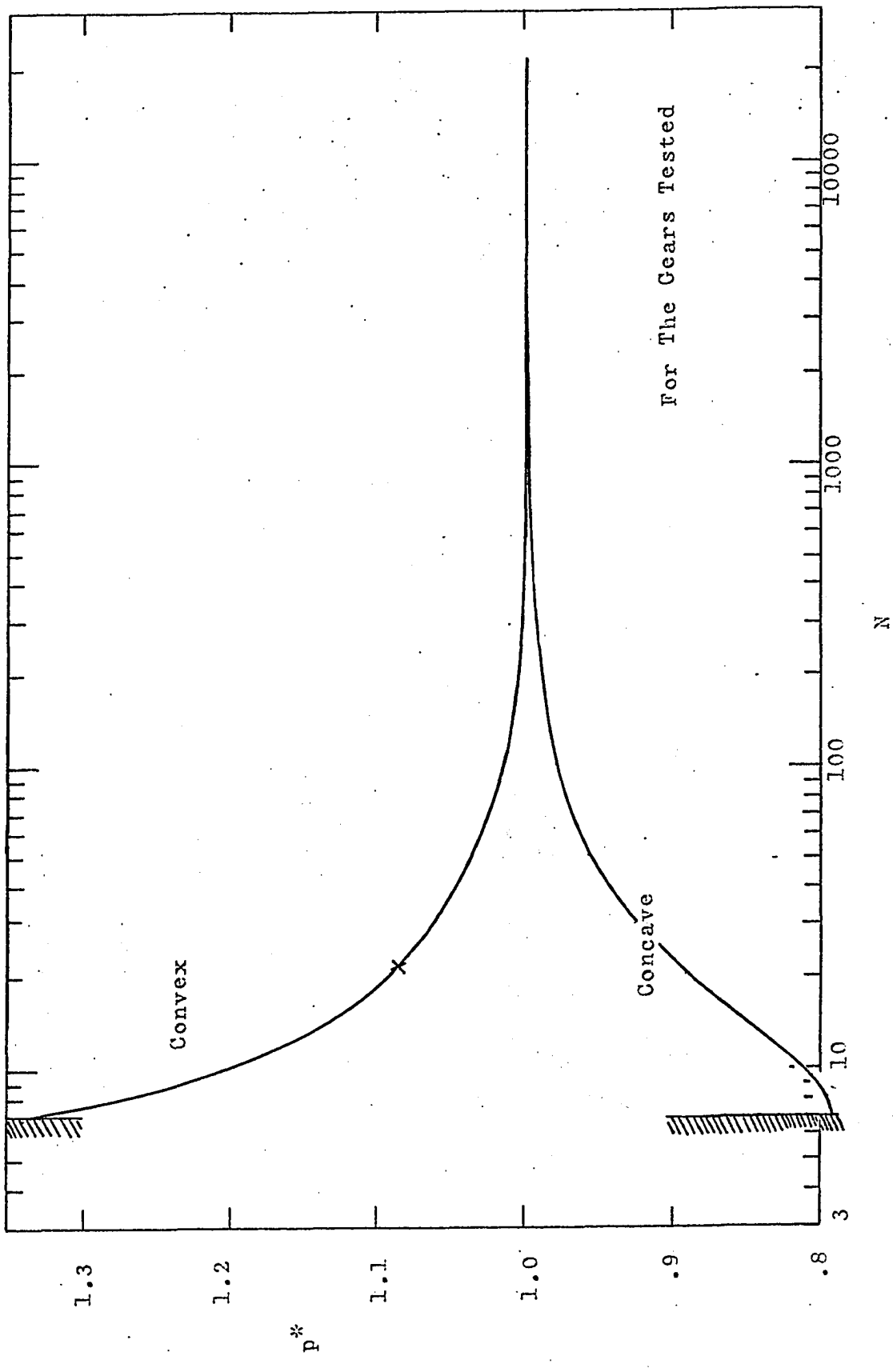

Reproduced with permission of the copyright owner. Further reproduction prohibited without permission.

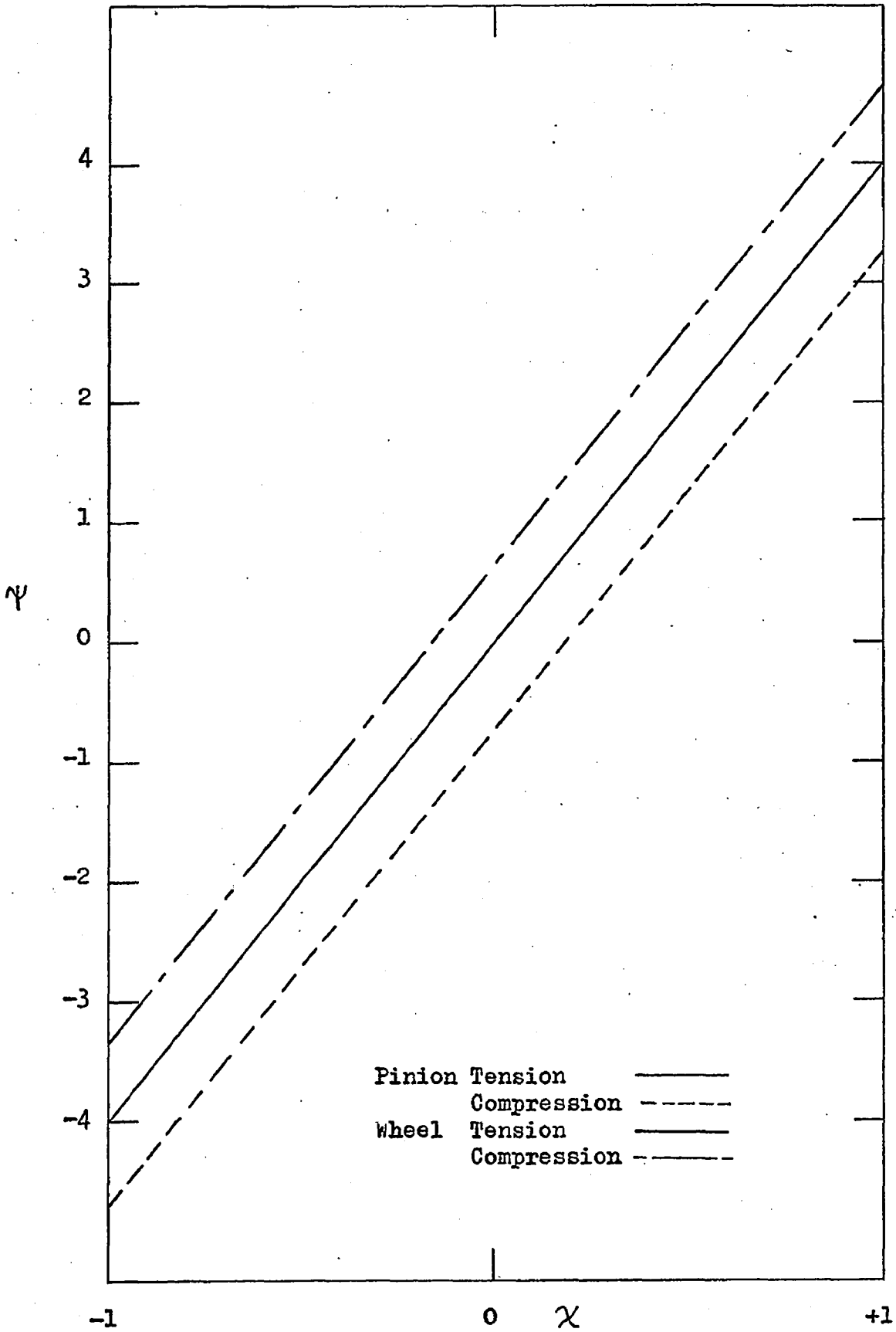

Fig. 7 Position of Load Along Tooth $\varkappa$ vs Angular Position Ψ

Reproduced with permission of the copyright owner. Further reproduction prohibited without permission.

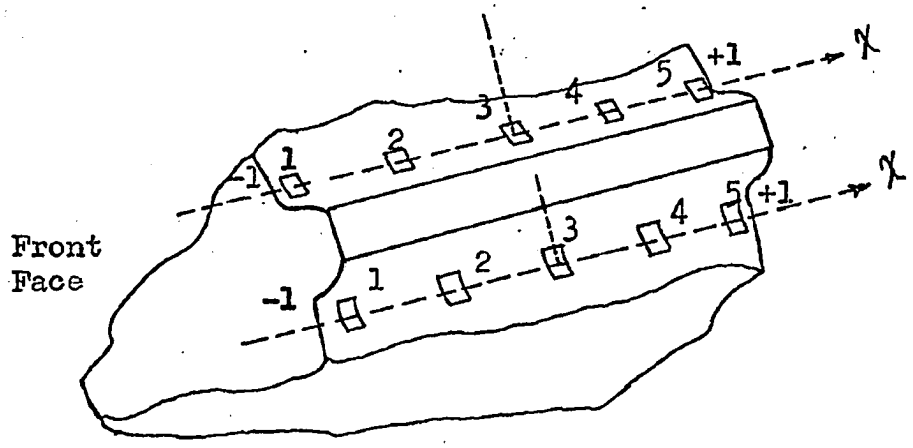

χ	Gage #				
	1	2	3	4	5
Pinion Tension	-.885	-.455	.145	.518	.950
Pinion Compression	-.914	-.484	-.050	.375	.860
Wheel Tension	-.885	-.484	.145	.488	.892
Wheel Compression	-.844	-.455	.000	.433	.892

Fig. 8 Strain Gage Locations
(Across Width of Tooth)

Reproduced with permission of the copyright owner. Further reproduction prohibited without permission.

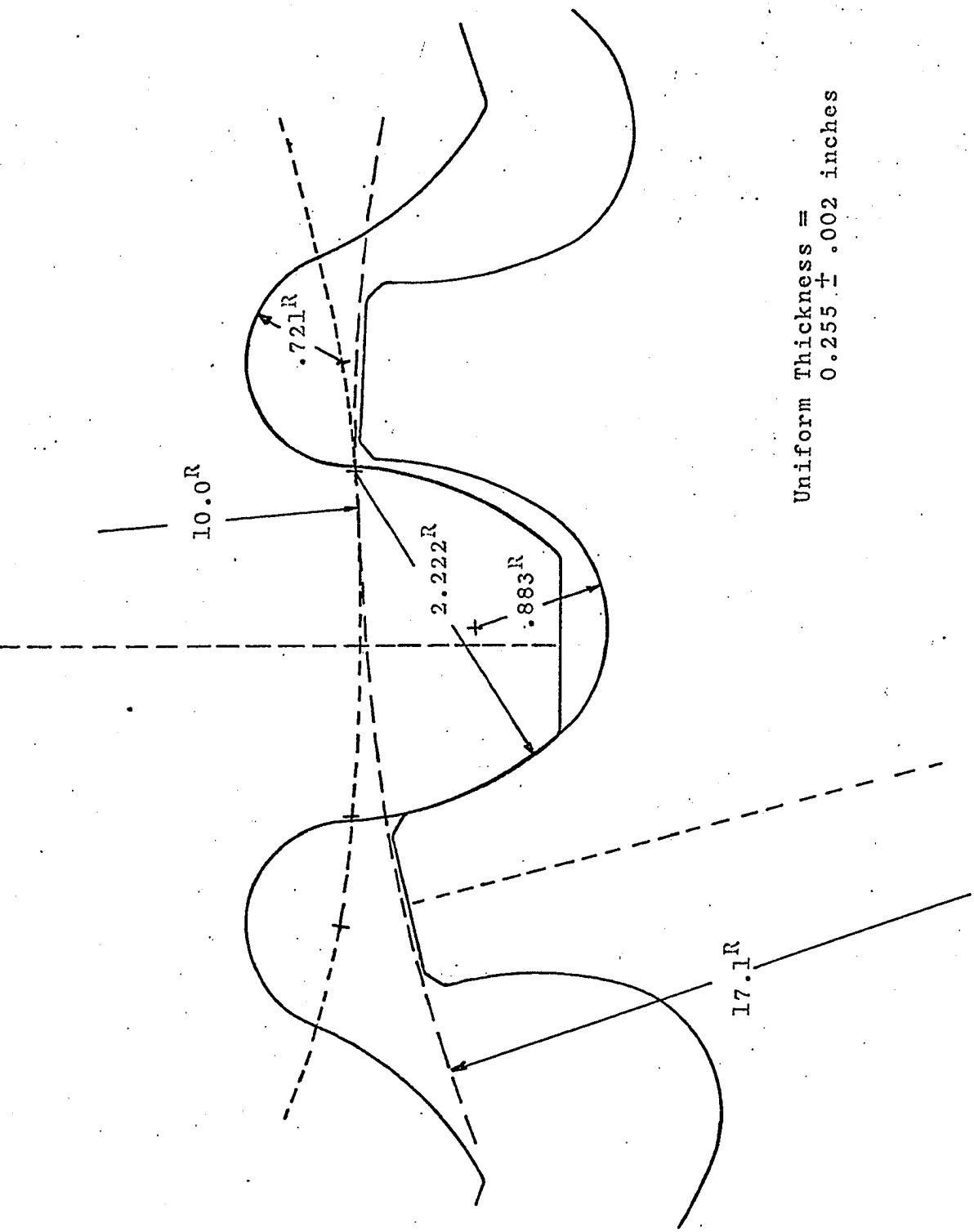

Fig. 9 Tooth Proportions For Photoelastic Model

Reproduced with permission of the copyright owner. Further reproduction prohibited without permission.

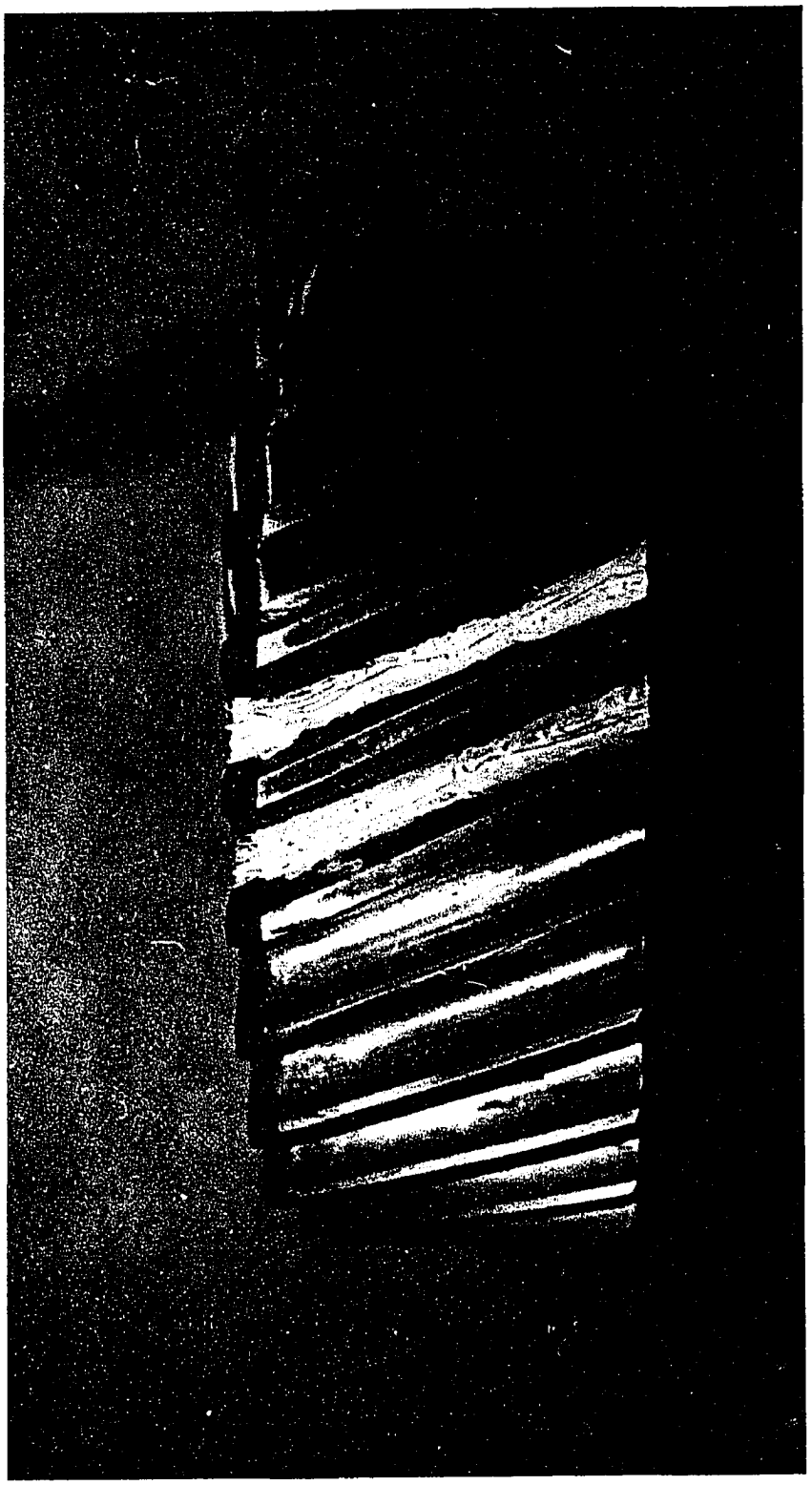

Fig. 10 Photostress and Strain Gages in Position on Wheel

Reproduced with permission of the copyright owner. Further reproduction prohibited without permission.

Fig. 11 Isochromatic Fringe Photograph : W_t=3030 lb. Pinion Tooth , Reflection Polariscope , Ψ=-4

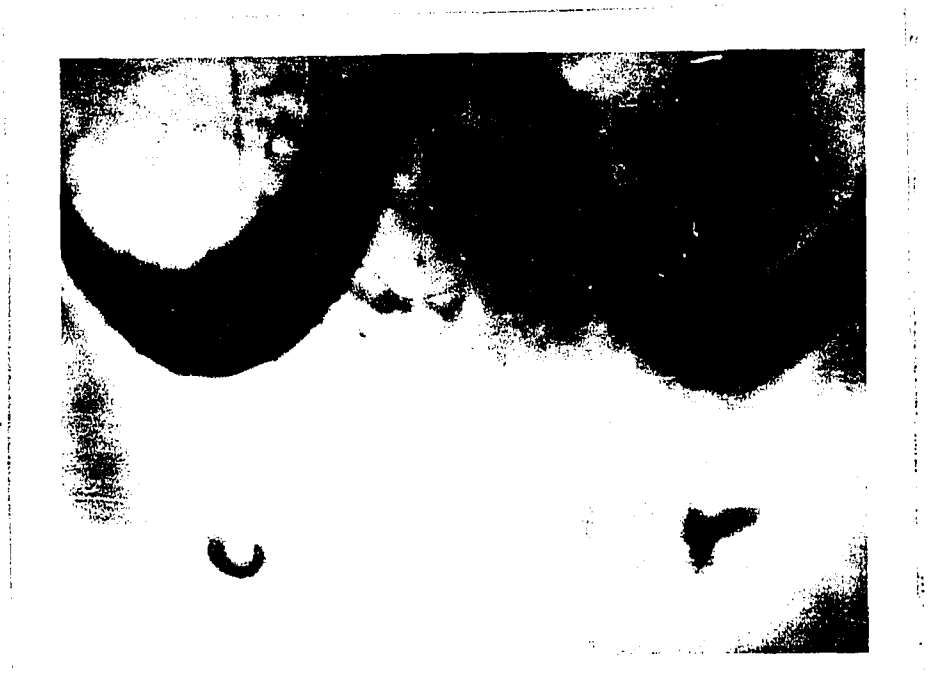

Fig. 12 Isochromatic Fringe Photograph : W_t=3030 lb. Wheel Tooth , Reflection Polariscope , Ψ=-4

Reproduced with permission of the copyright owner. Further reproduction prohibited without permission.

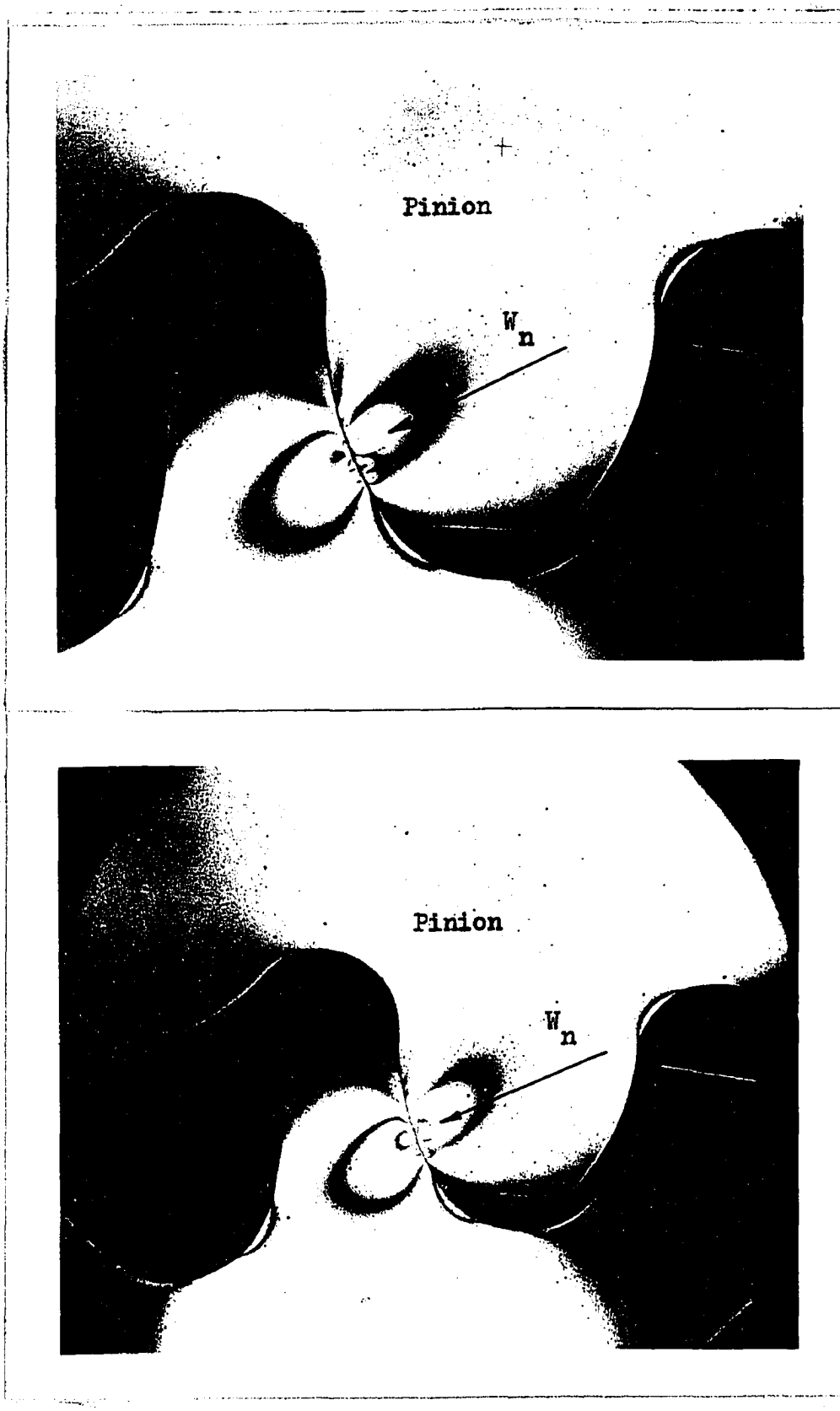

Fig. 13 Isochromatic Fringe Photograph : W_n=27.9 lb.
(Transmission Polariscope)

Reproduced with permission of the copyright owner. Further reproduction prohibited without permission.

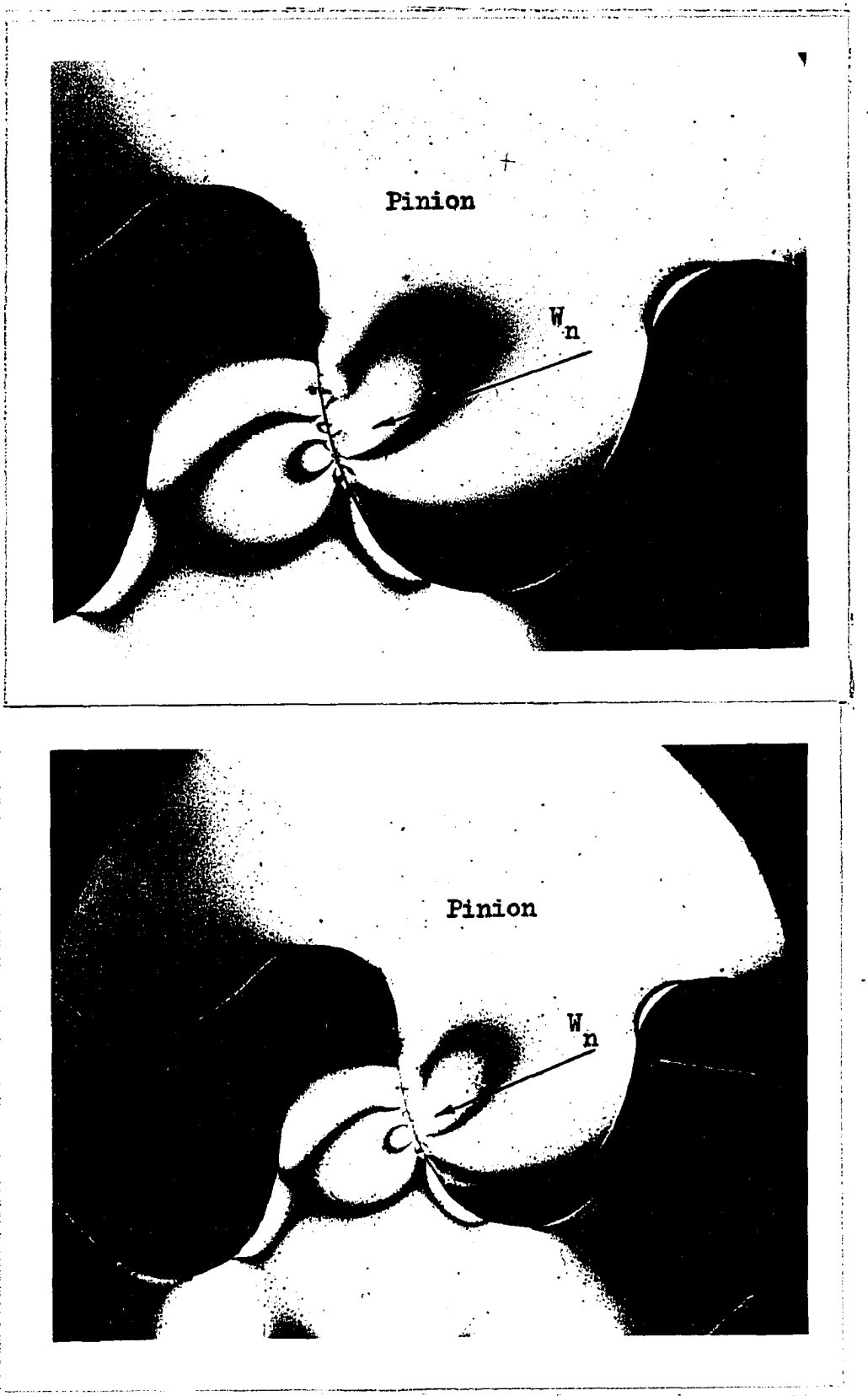

Fig.14 Isochromatic Fringe Photograph :W_n=34.9 lb.
(Transmission Polariscope)

Reproduced with permission of the copyright owner. Further reproduction prohibited without permission.

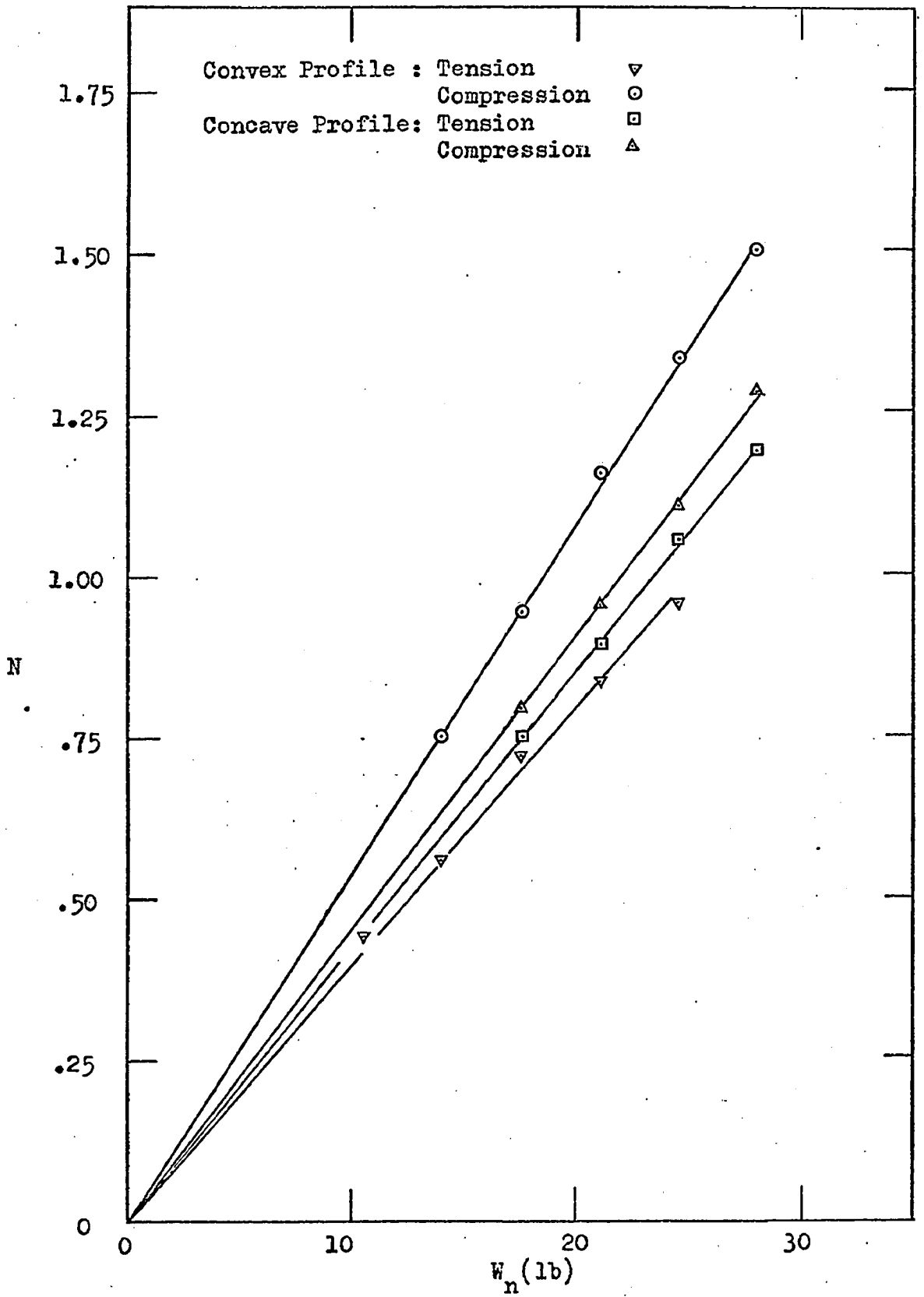

Fig. 15 Fringe Order N vs Normal Load W_n
2-D Photoelastic Model

Reproduced with permission of the copyright owner. Further reproduction prohibited without permission.

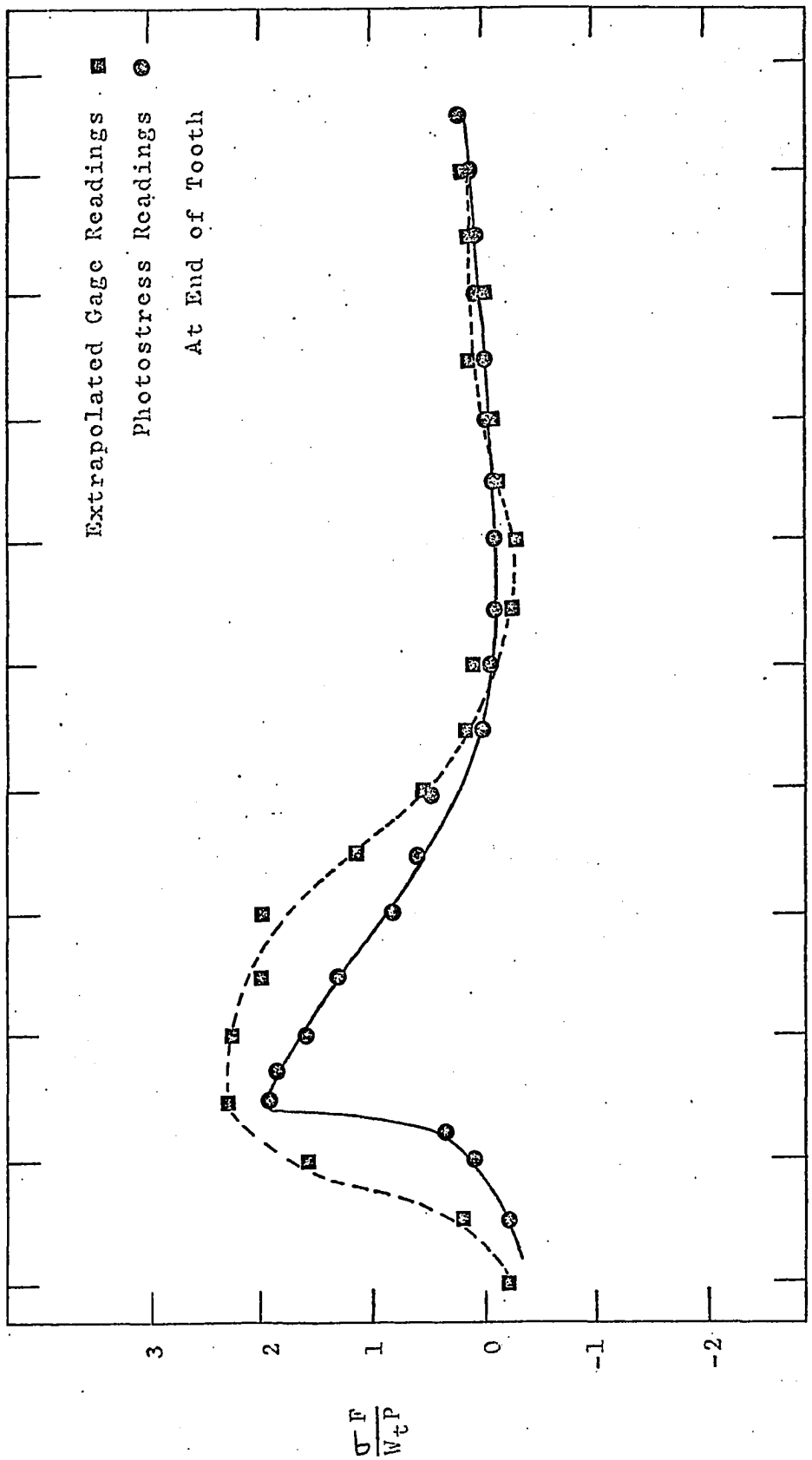

Fig. 16 $\frac{\sigma F}{W_t P}$ vs Angular Position ψ : Pinion Tension

Reproduced with permission of the copyright owner. Further reproduction prohibited without permission.

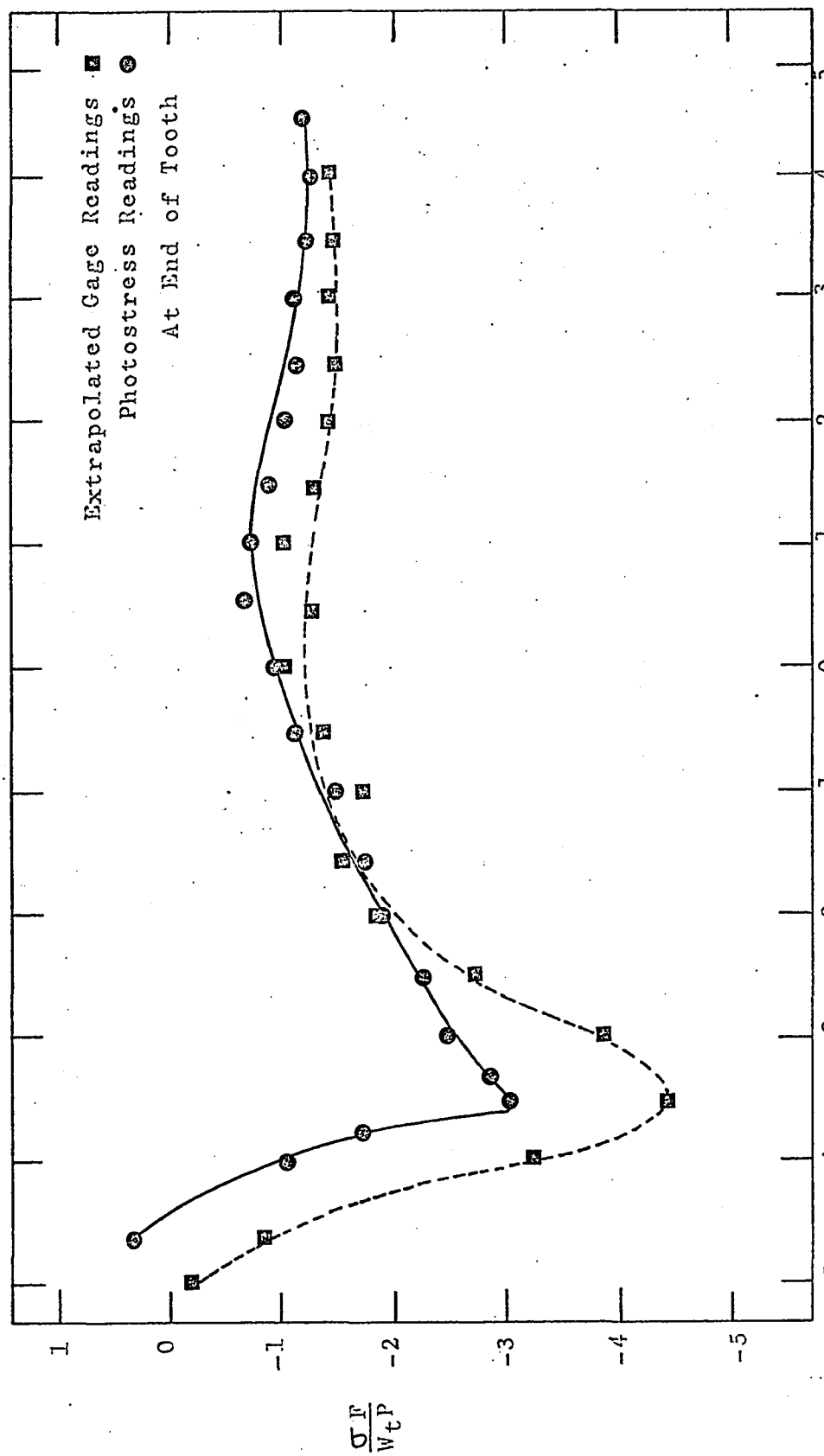

Fig. 17 $\frac{\sigma F}{W_t P}$ vs Angular Position ψ : Pinion Compression

Reproduced with permission of the copyright owner. Further reproduction prohibited without permission.

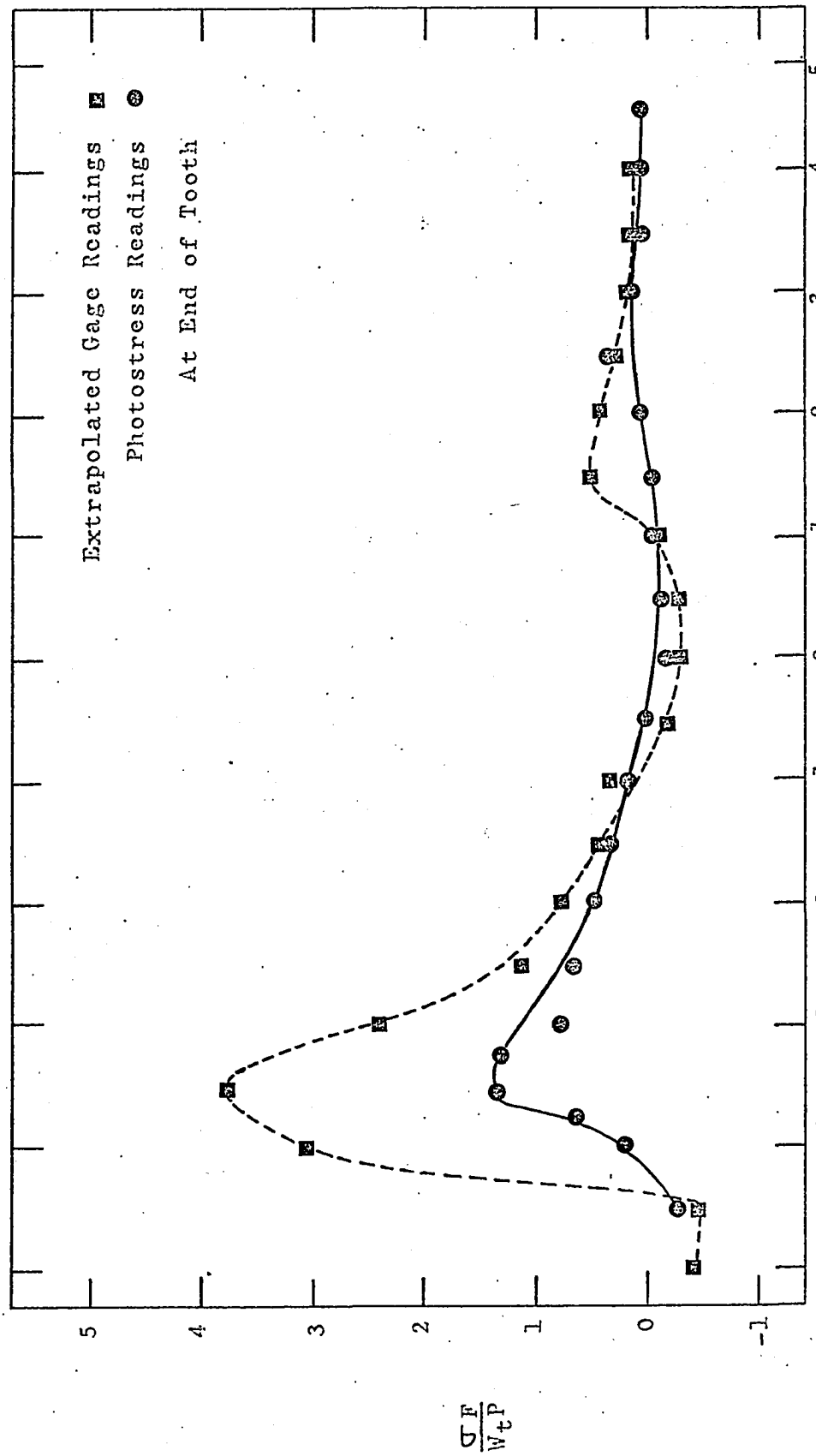

Fig. 18 $\frac{\sigma F}{W_t P}$ vs Angular Position Ψ : Wheel Tension

Reproduced with permission of the copyright owner. Further reproduction prohibited without permission.

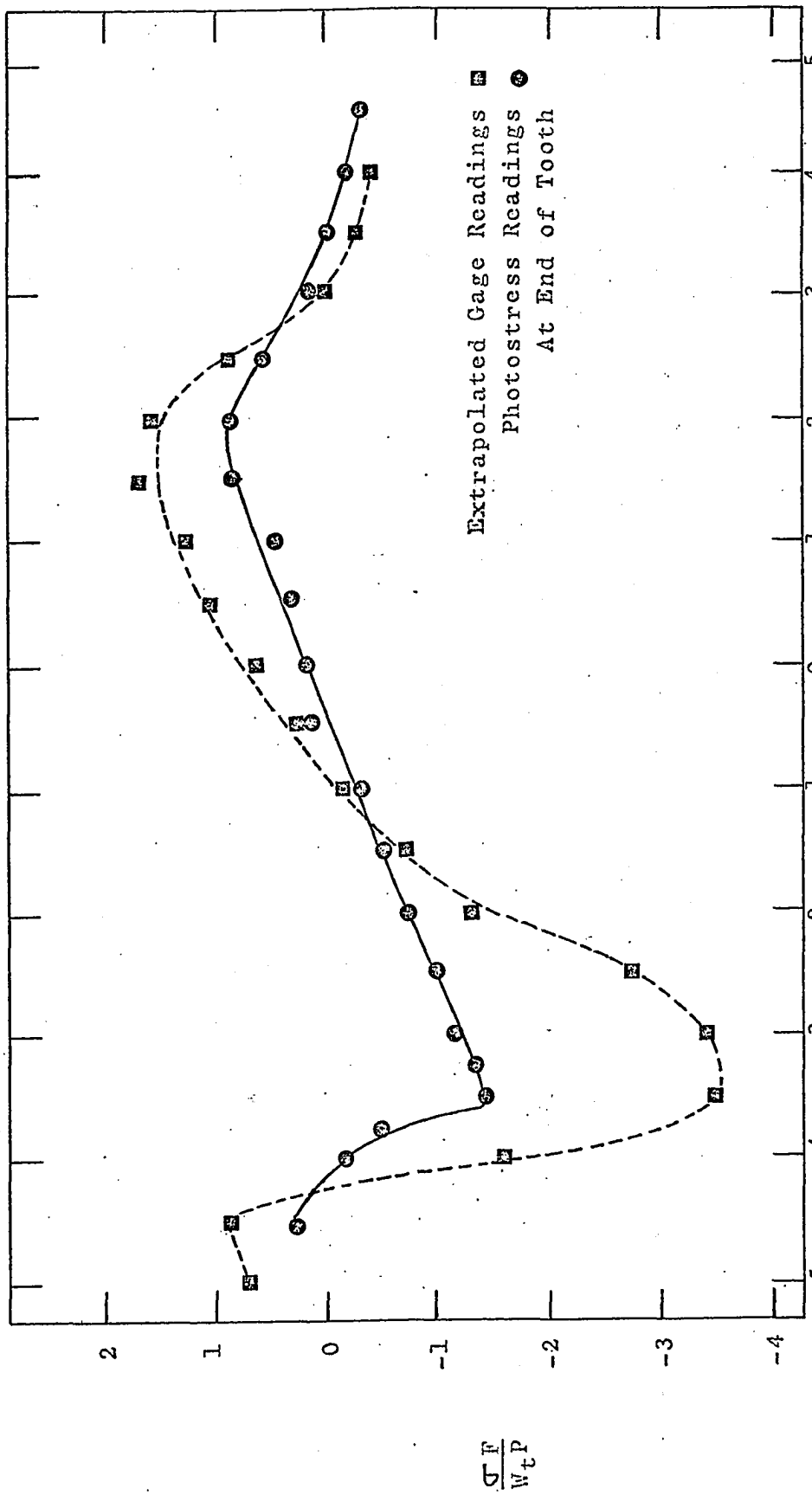

Fig. 19 $\frac{\sigma F}{W_t P}$ vs Angular Position ψ : Wheel Compression

Reproduced with permission of the copyright owner. Further reproduction prohibited without permission.

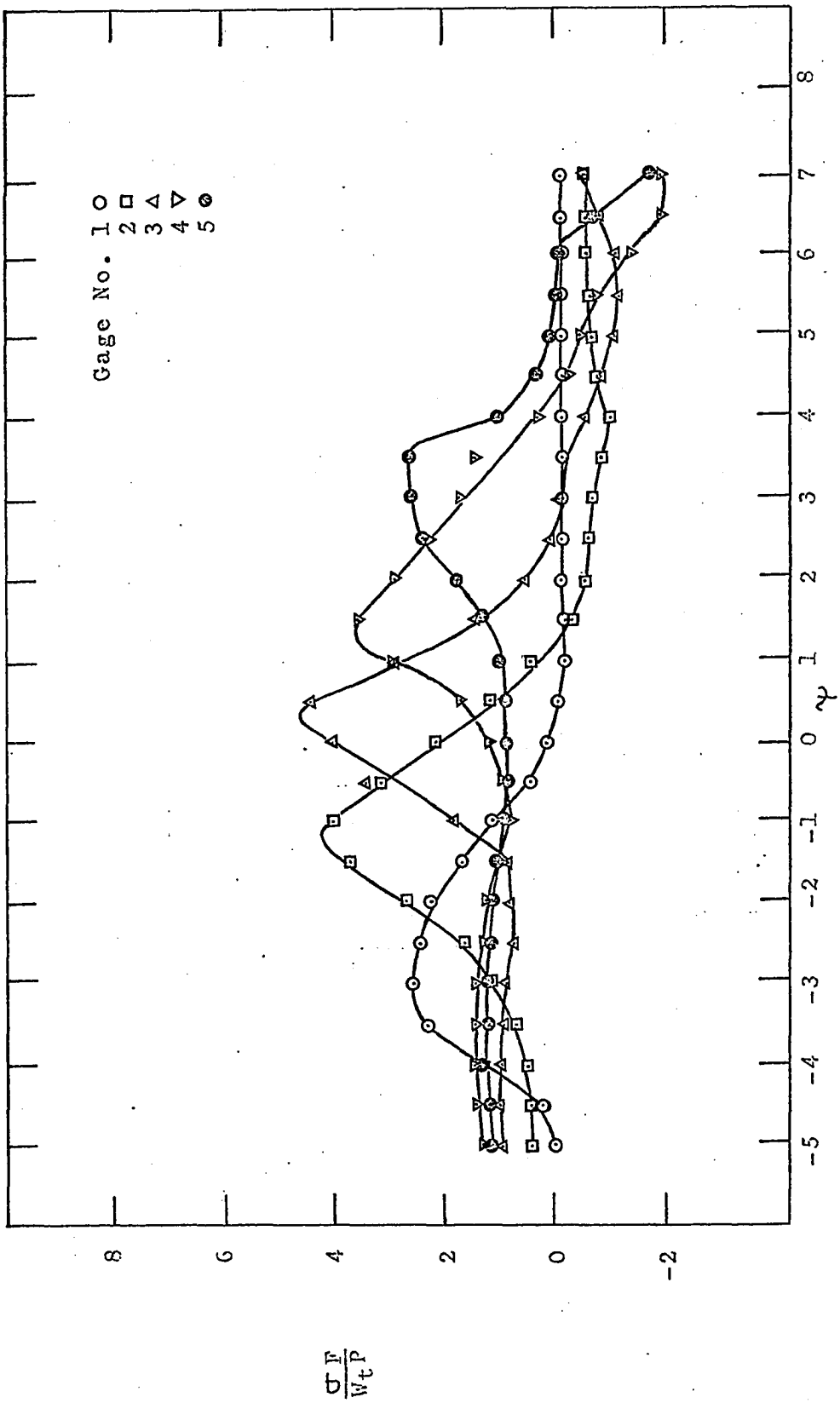

Fig. 20 $\frac{\sigma F}{W_t P}$ vs Angular Position ψ : Pinion Tension Strain Gage Test

Reproduced with permission of the copyright owner. Further reproduction prohibited without permission.

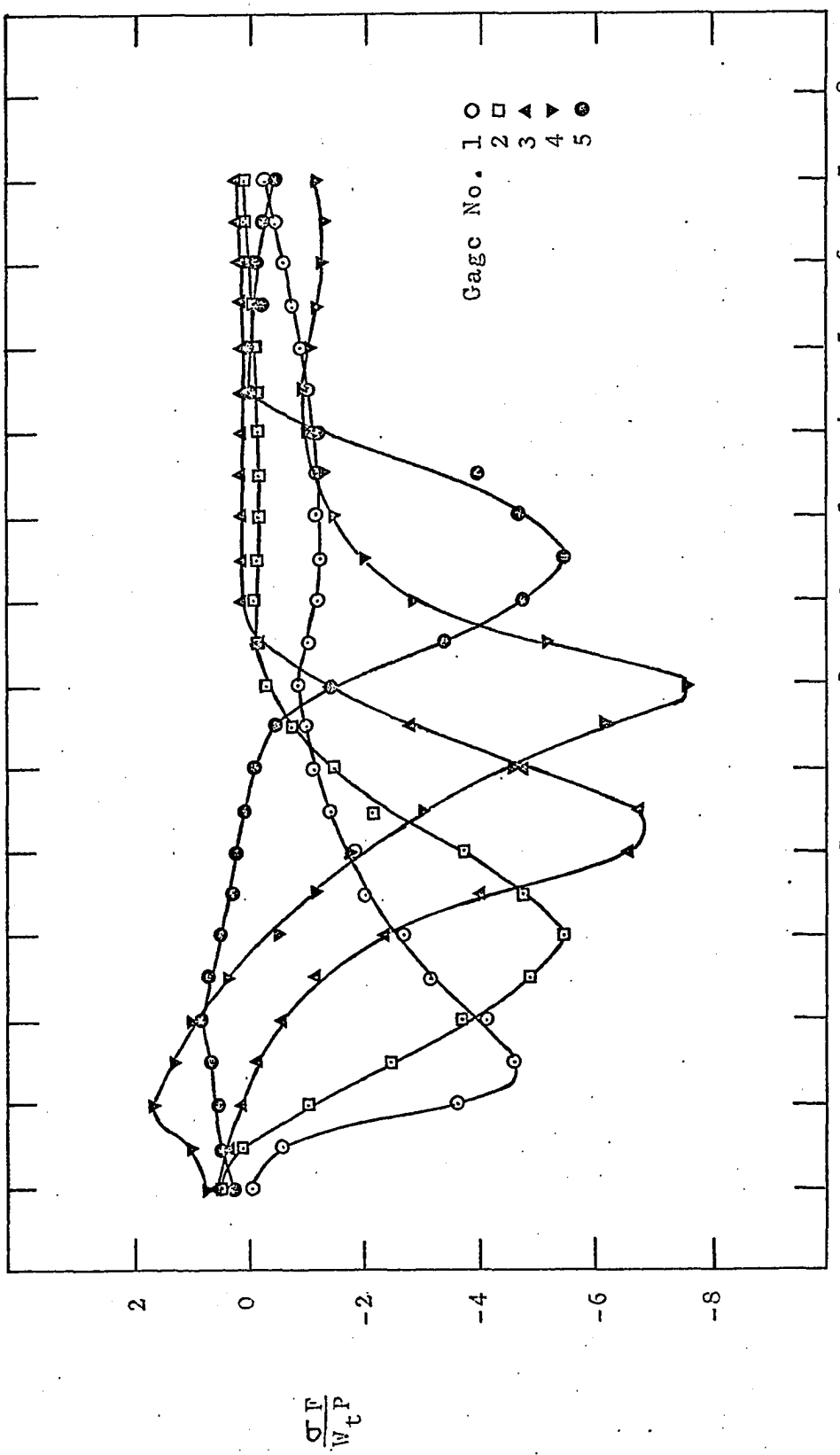

Fig. 21 $\frac{\sigma_F}{W_t P}$ vs Angular Position ψ : Pinion Compression Strain Gage Tests

Reproduced with permission of the copyright owner. Further reproduction prohibited without permission.

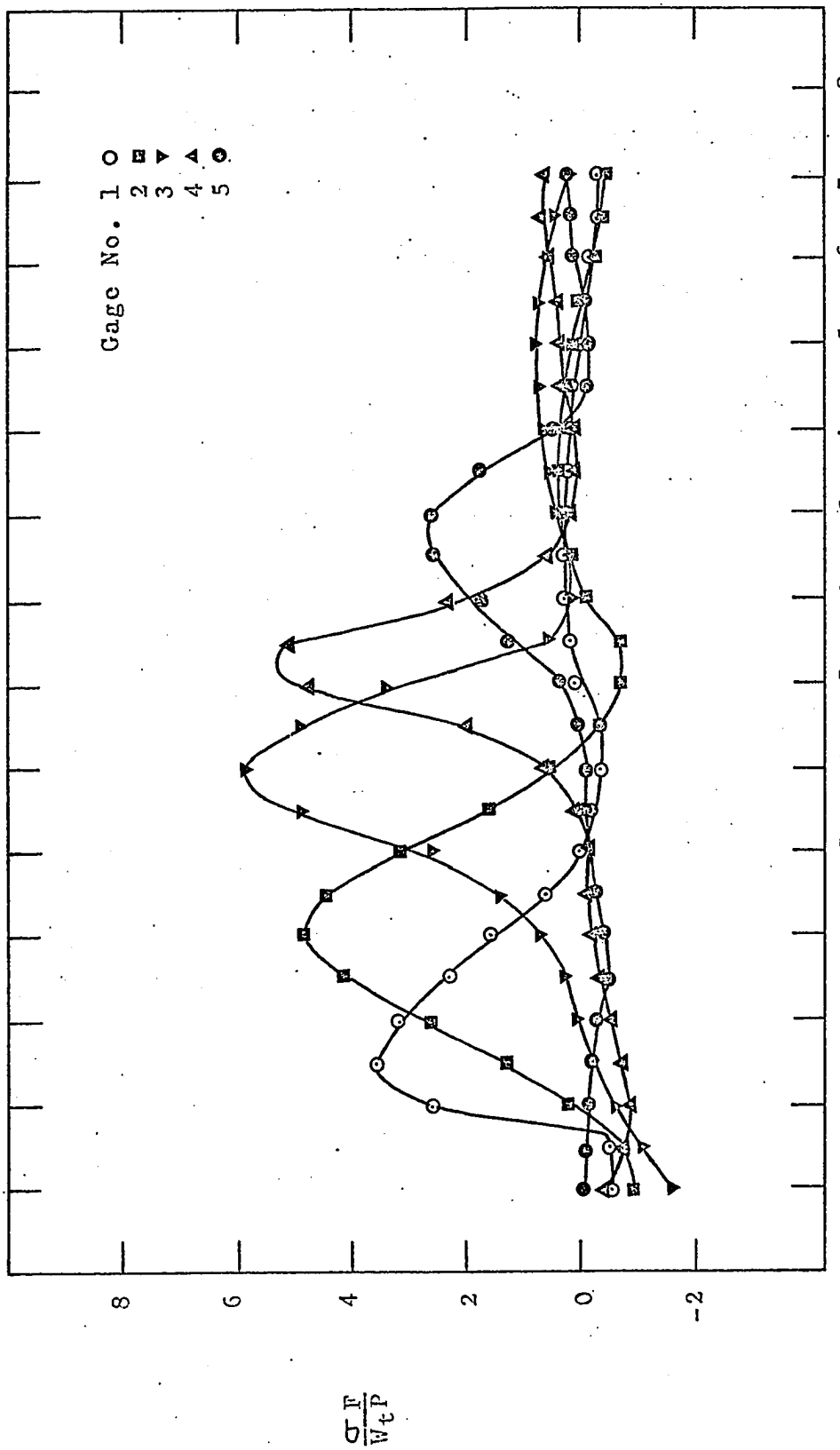

Fig. 22 $\frac{\sigma F}{W_t P}$ vs Angular Position ψ : Wheel Tension Strain Gage Test

Reproduced with permission of the copyright owner. Further reproduction prohibited without permission.

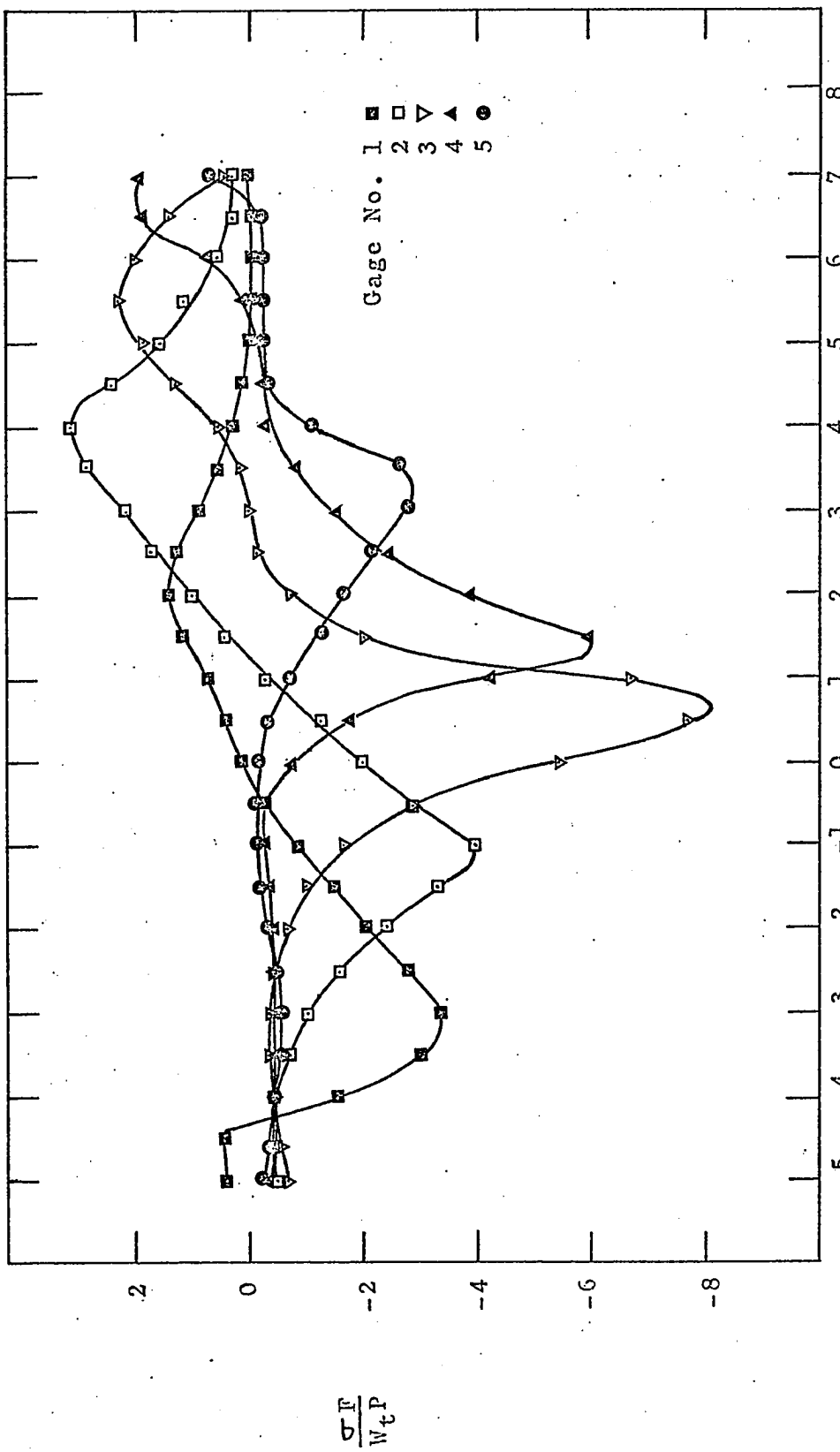

Fig. 23 $\frac{\sigma F}{W_t P}$ vs Angular Position ψ : Wheel Compression Strain Gage Test

Reproduced with permission of the copyright owner. Further reproduction prohibited without permission.

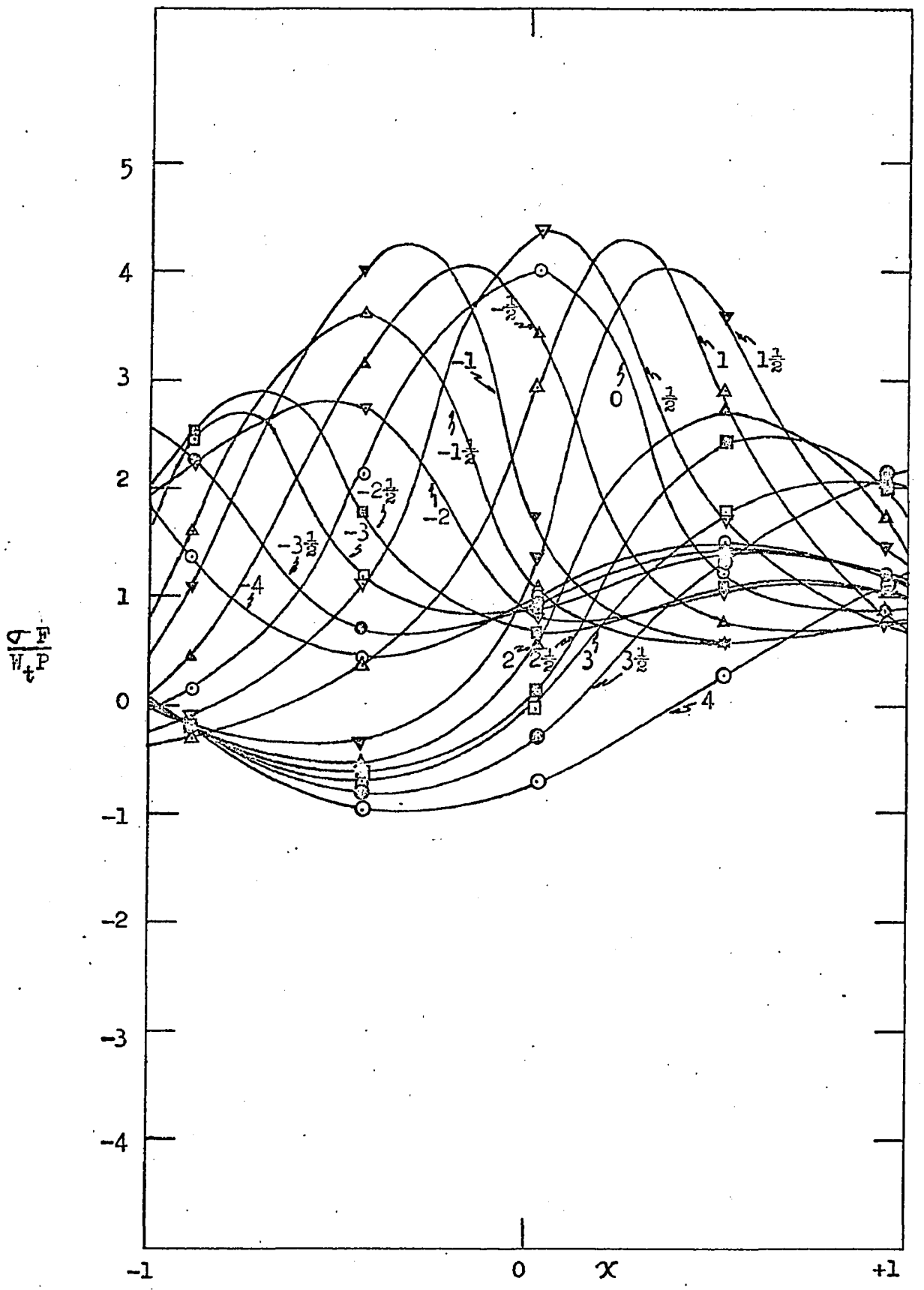

Fig. 24 $\frac{\sigma F}{W_t P}$ vs Distance Along Tooth X

For Various Values of Y
Pinion Tension

Reproduced with permission of the copyright owner. Further reproduction prohibited without permission.

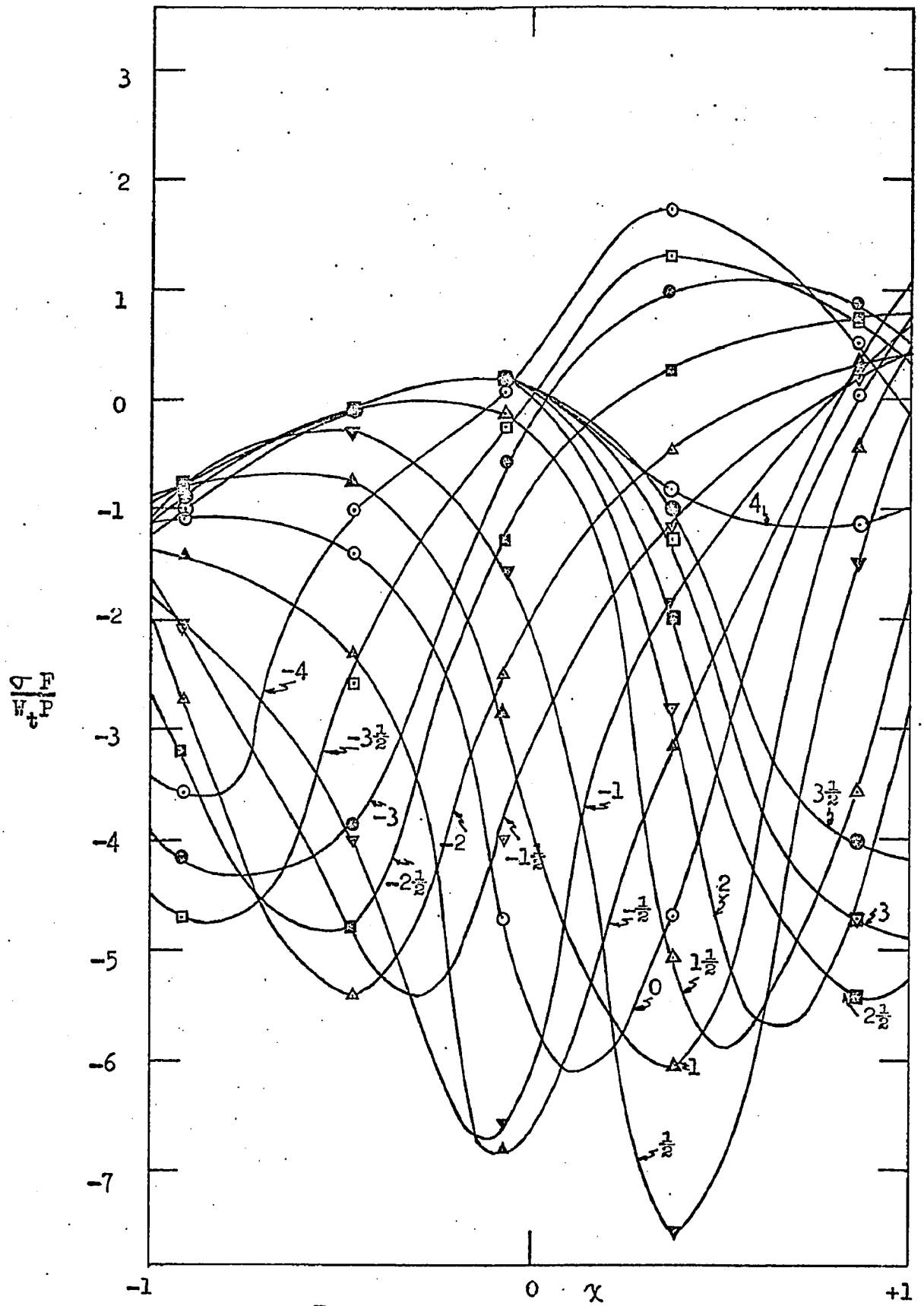

Fig.25 $\frac{\sigma F}{W_t P}$ vs Distance Along Tooth x

For Various Values of ψ
Pinion Compression

Reproduced with permission of the copyright owner. Further reproduction prohibited without permission.

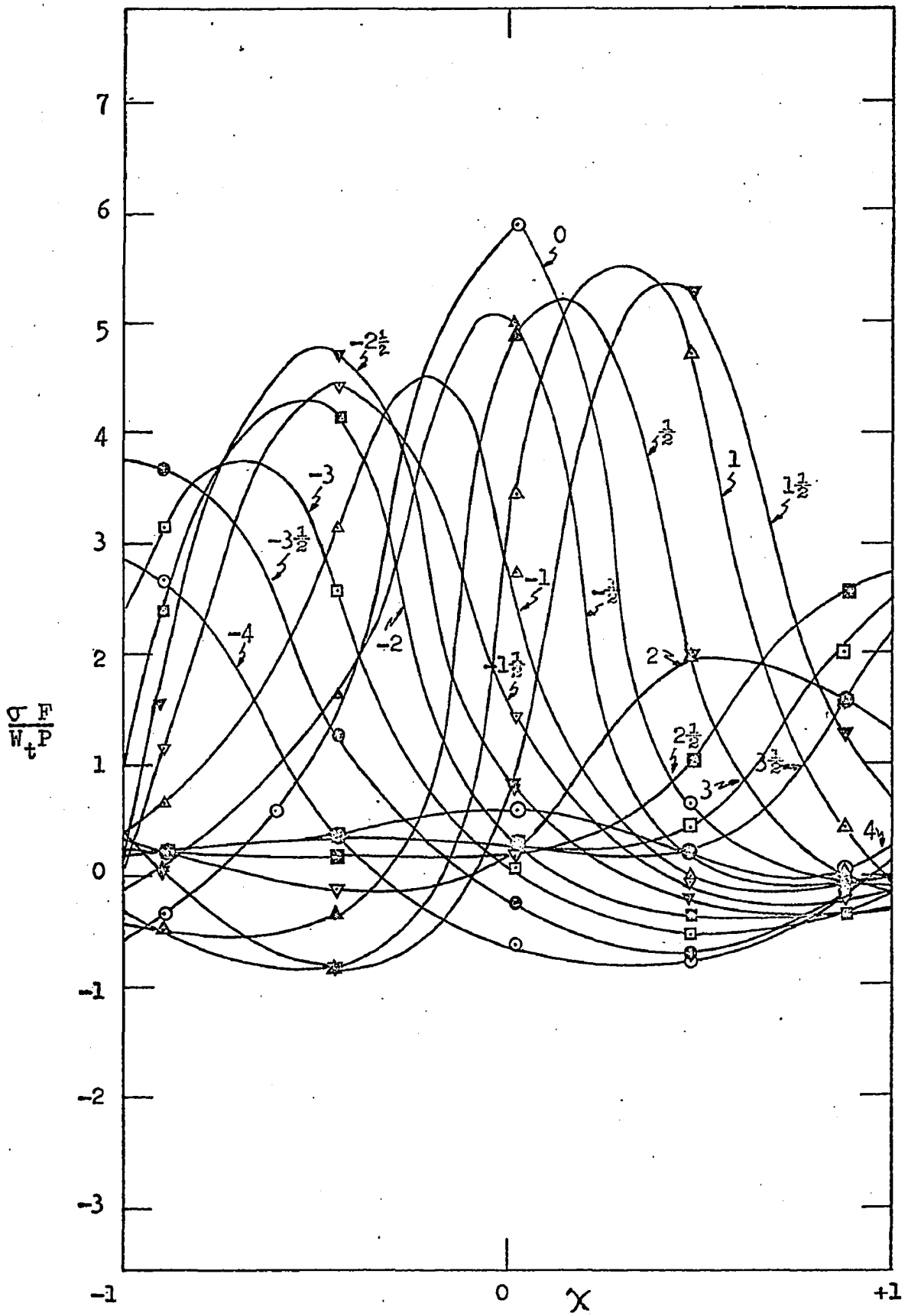

Fig. 26 $\frac{\sigma F}{W_t P}$ vs Distance Along Tooth χ

For Various Values of γ

Wheel Tension

Reproduced with permission of the copyright owner. Further reproduction prohibited without permission.

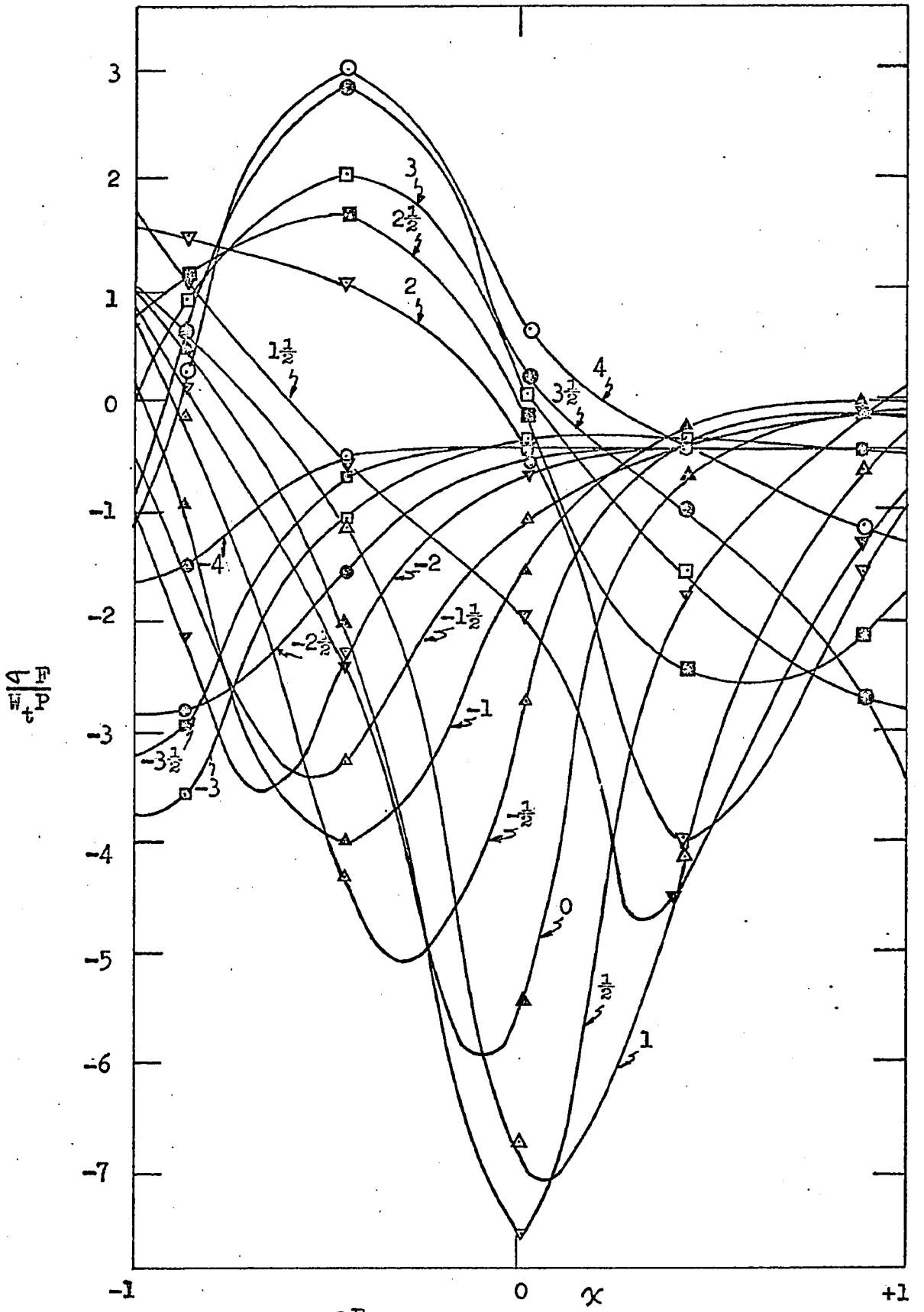

Fig. 27 $\frac{\sigma F}{W_t P}$ vs Distance Along Tooth χ

For Various Values of Ψ
Wheel Compression

Reproduced with permission of the copyright owner. Further reproduction prohibited without permission.

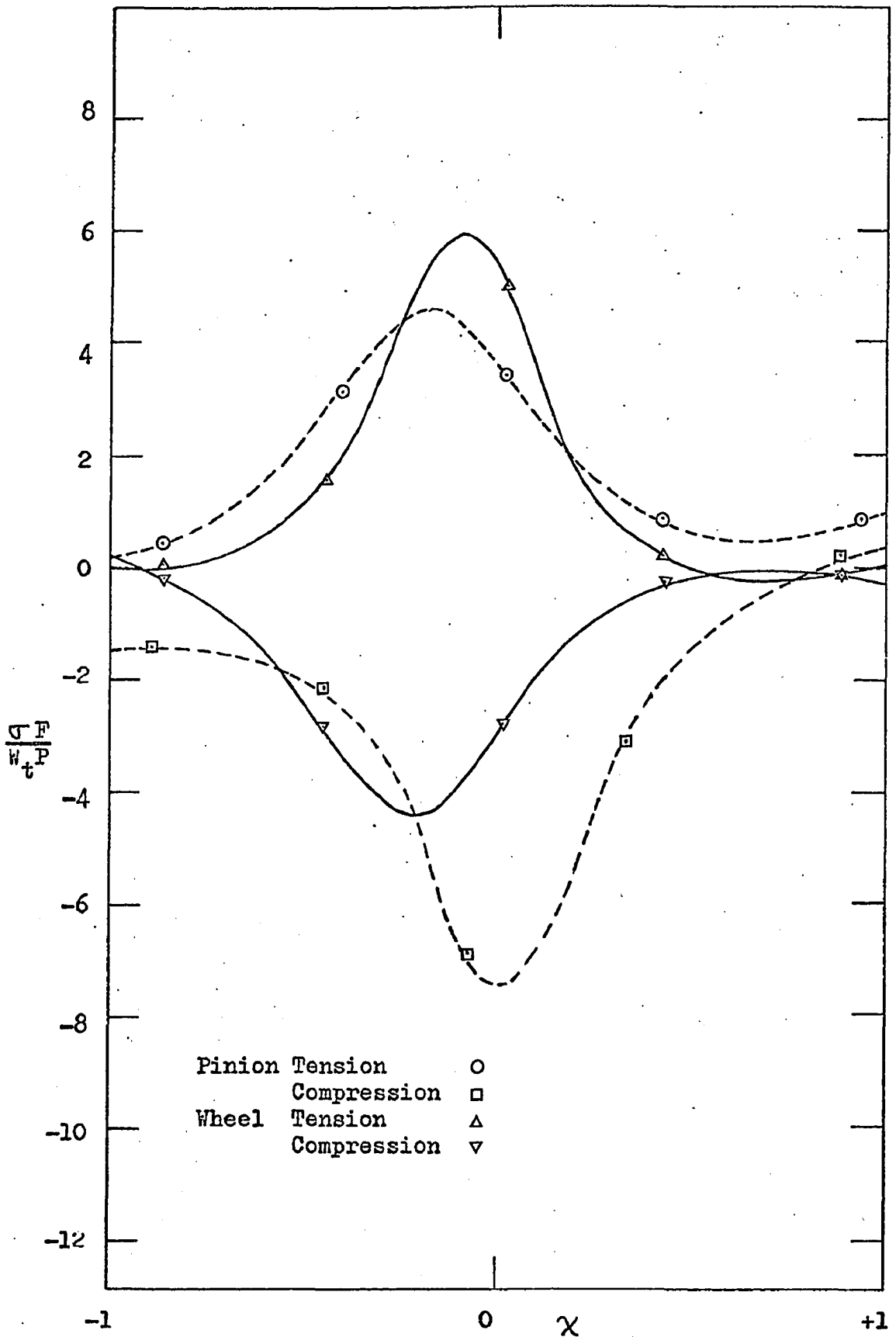

Fig. 28 $\frac{\sigma F}{W_t P}$ vs Distance Along Tooth χ
For $\Psi = -\frac{1}{2}$

Reproduced with permission of the copyright owner. Further reproduction prohibited without permission.

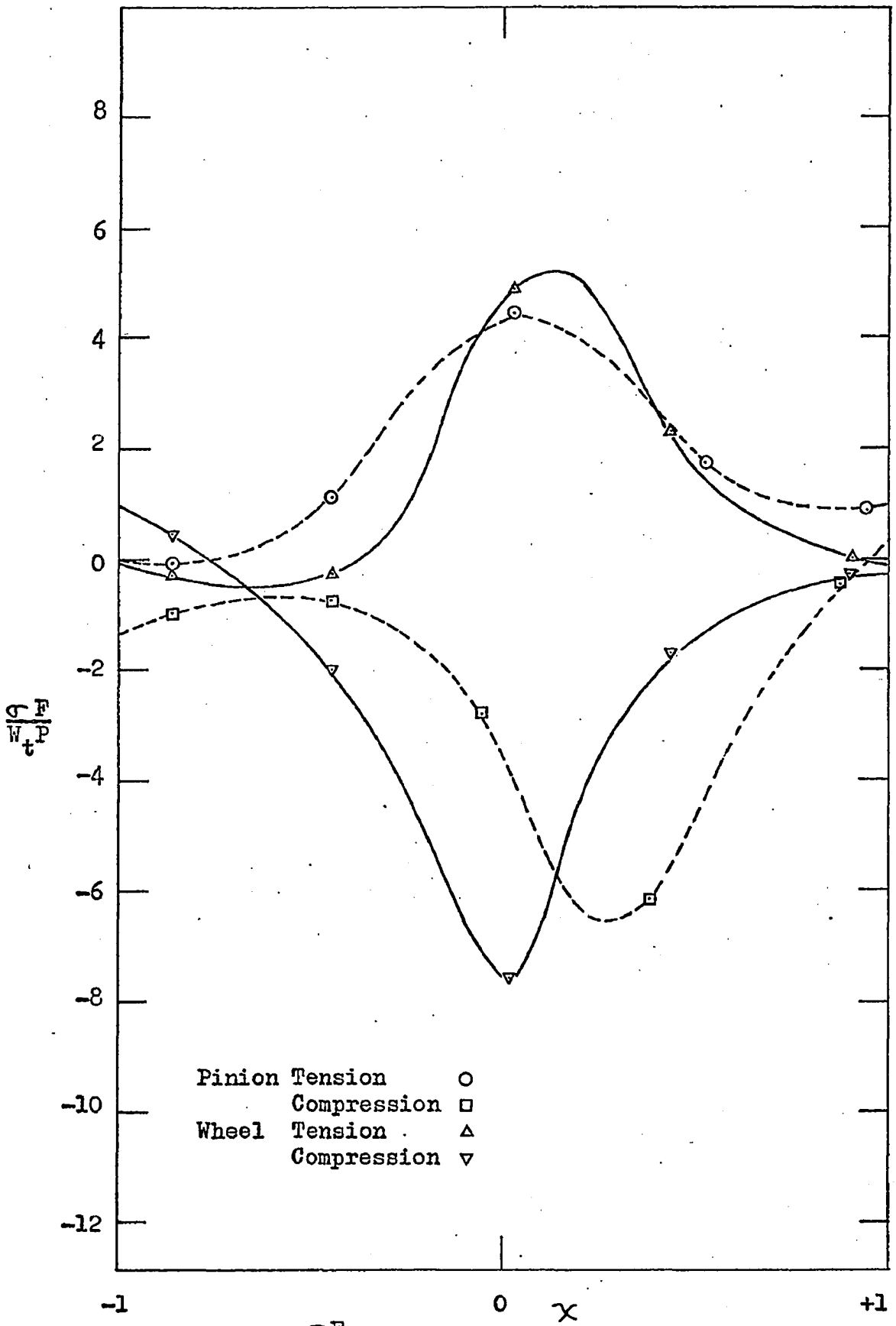

Fig. 29 $\frac{\sigma F}{W_t P}$ vs Distance Along Tooth χ
For $\Psi = \frac{1}{2}$

Reproduced with permission of the copyright owner. Further reproduction prohibited without permission.

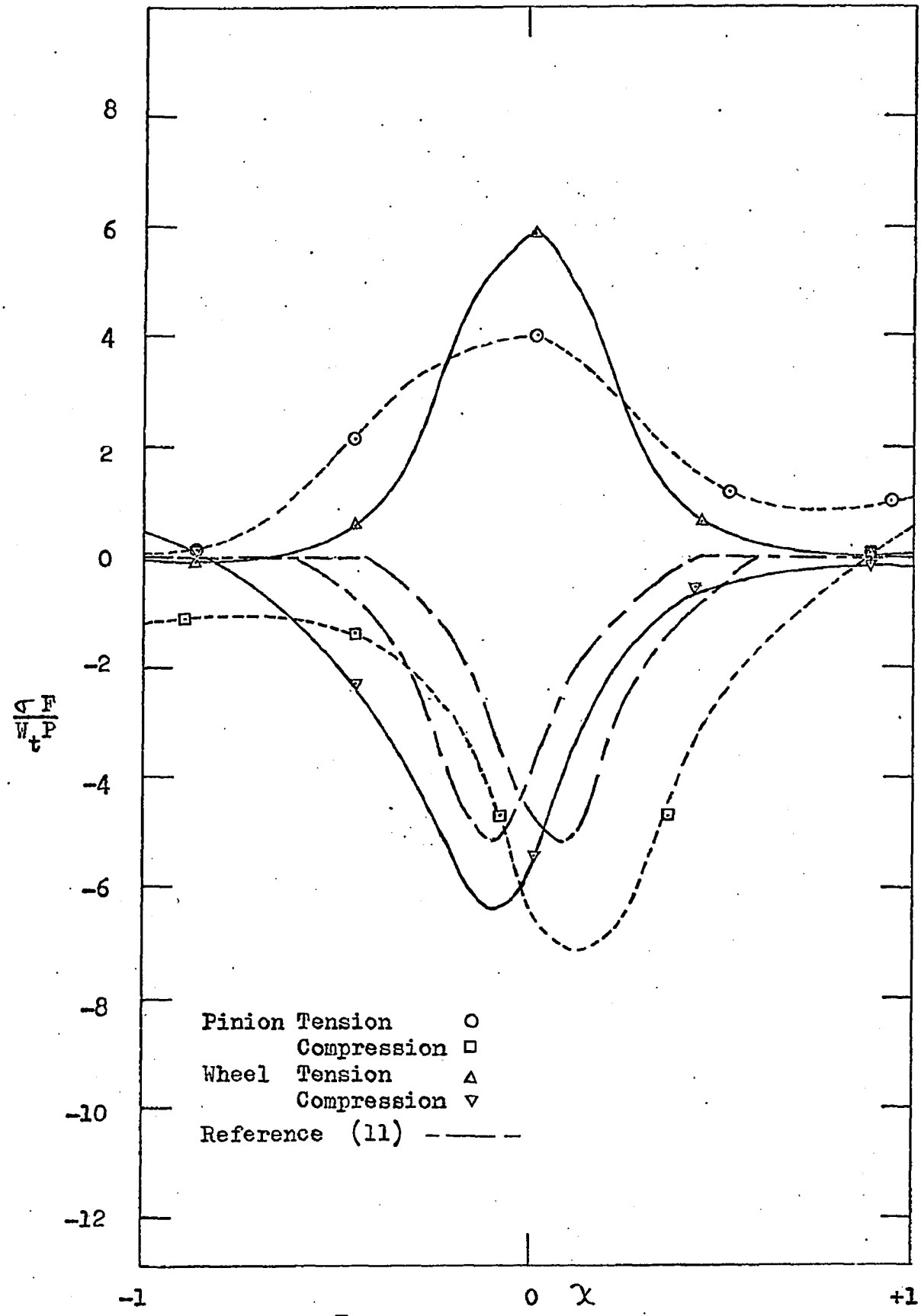

Fig. 30 $\frac{\sigma F}{W_t P}$ vs Distance Along Tooth χ

For $\gamma = 0$

Reproduced with permission of the copyright owner. Further reproduction prohibited without permission.

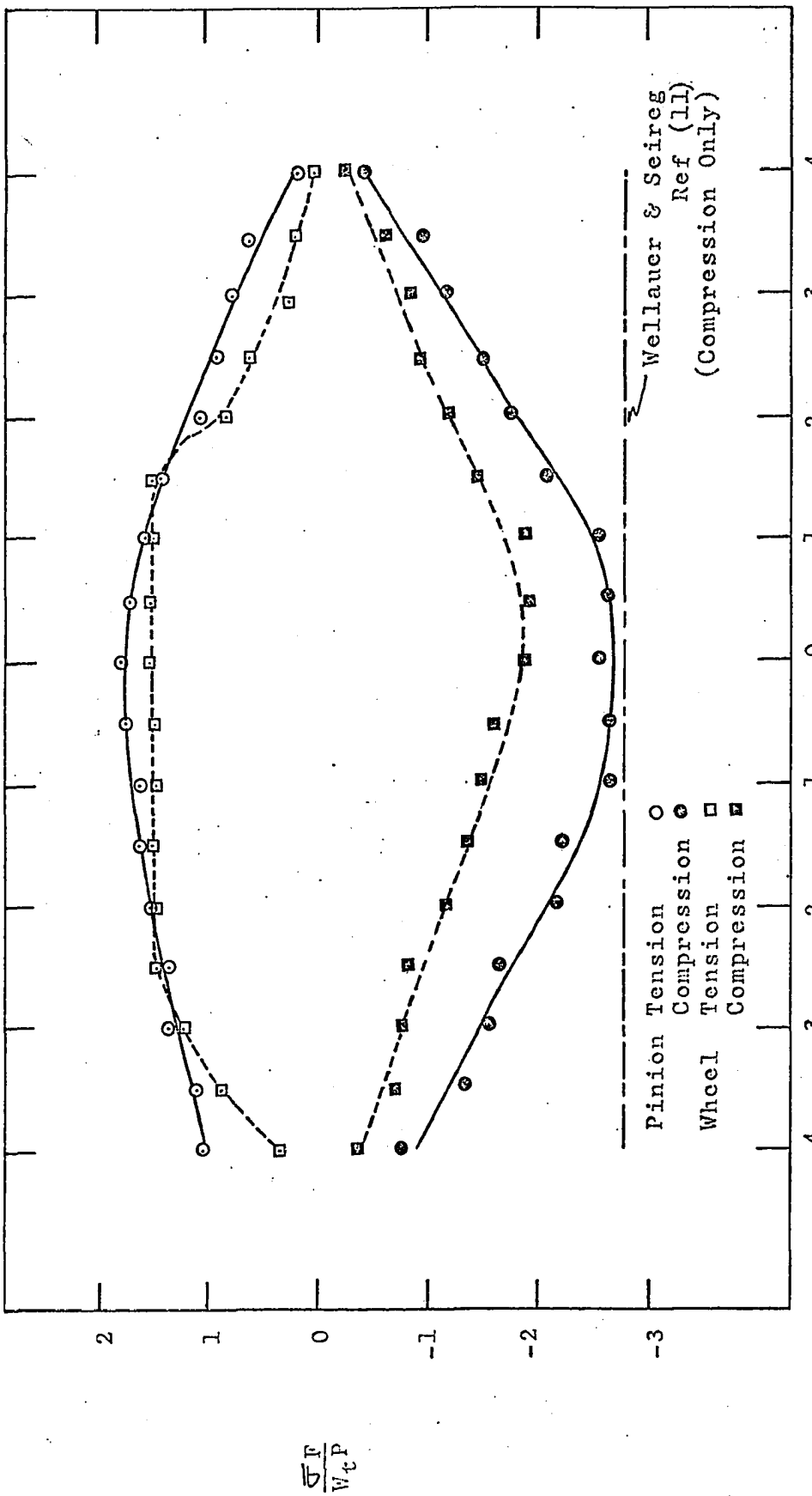

Fig. 31 Average Stress Intensity $\frac{\sigma F}{W_t P}$ vs Angular Rotation ψ

Reproduced with permission of the copyright owner. Further reproduction prohibited without permission.

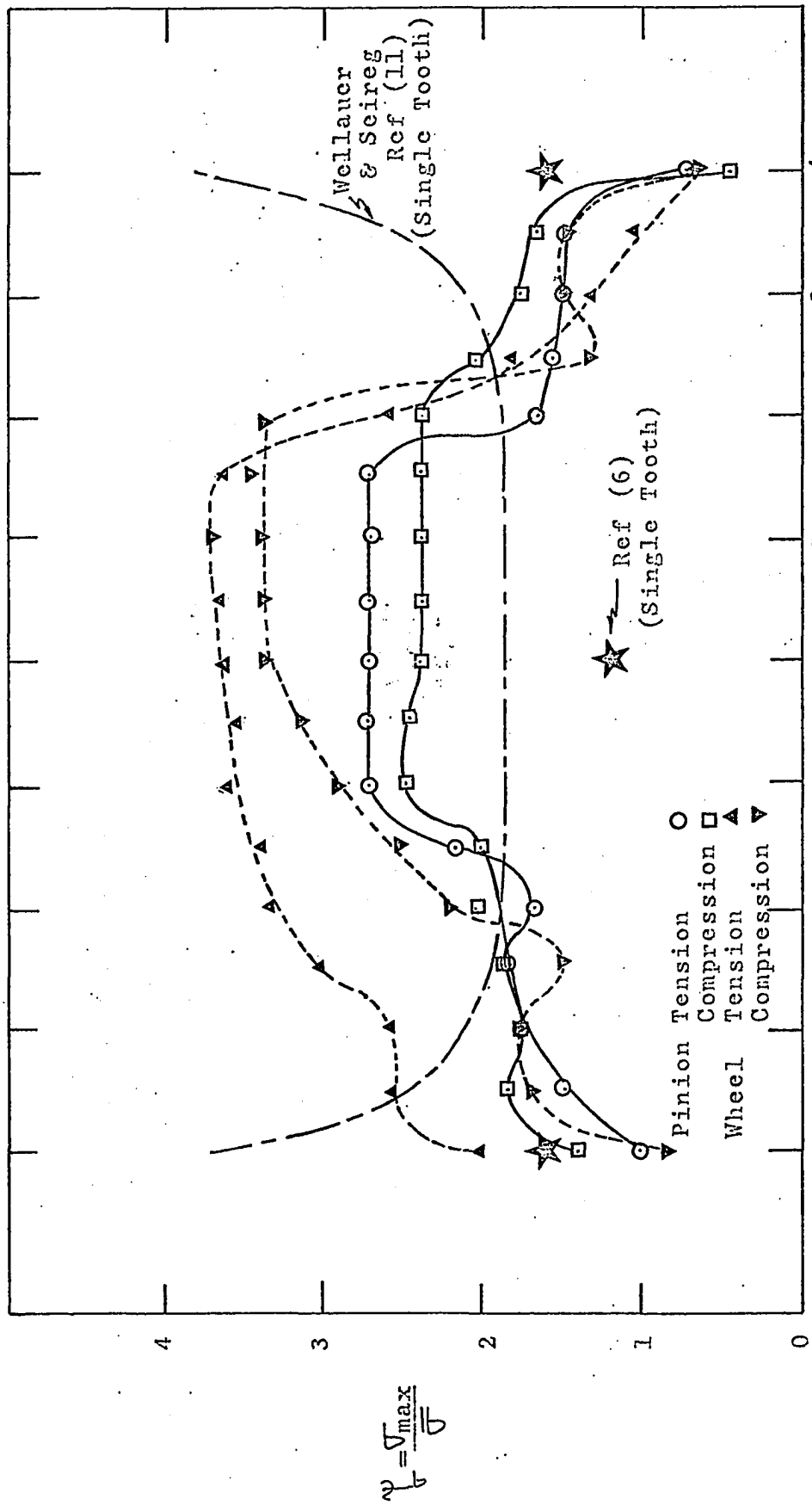

Fig. 32 Stress Distribution Factor ψ_σ vs Angular Rotation ψ

Reproduced with permission of the copyright owner. Further reproduction prohibited without permission.

	Experimental		Wellauer and Siereg (11)	Fedyakin and Chesnokov (5)
	2-D	3-D		
Pinion Tension	.923	1.07	———	———
Pinion Comp.	1.25	1.45	1.60	1.45
Wheel Tension	1.33	1.23	———	———
Wheel Comp.	1.42	1.53	2.15	1.66

Fig. 33 Values of the Stress Concentration Factor K as Determined from Experiment and References (11) and(5)

	Experimental	Wellauer and Siereg (11)	Fedyakin and Chesnokov (5)
Pinion Tension	2.6	1.8	1.2
Pinion Comp.	2.4	"	"
Wheel Tension	3.7	"	"
Wheel Comp.	3.4	"	"

Fig. 34 Values of Ψ_σ for System Studied, $\Upsilon = 0$

Reproduced with permission of the copyright owner. Further reproduction prohibited without permission.

APPENDIX A

GEAR LOADING FRAME

The gear loading frame serves two purposes:

1) apply the load to the teeth being studied
2) maintain the gears in proper orientation

The torque is applied to the gears, (which are keyed to two shafts) by a hydraulic jack. This jack has a maximum load rating of 6000 lb. The jack has its lower end fixed to a pivot which is connected to the two pieces of 8 inch channel which carry the loads and form the base of the frame. The upper end is pin connected to a lever arm (10 inches in length), which is keyed to the same shaft as the wheel. The shaft which the pinion is on is keyed to an arm as well and this arm is attached to the channel by means of an adjusting screw. The loading frame and its various components are shown in figure 35. The gears are mounted on cantilevered shafts so that the front end is exposed to the reflection polariscope and is freely accessible.

The shaft lengths were kept short (10") to prevent large deflections. This and the shaft diameter of $2\frac{1}{4}$ inches kept shaft deflection to less than 0.001 inches. The bearings for the shafts were cut from a solid block of steel so that the exact centre distance was maintained. The fit between the shafts and bearings was held to a very close tolerance in order to minimize movement under loading. This leads to large load losses due to friction which then requires further calibration.

The load is monitored by means of strain gages mounted on the input lever arm. Four gages are employed in a 4 arm strain gage bridge which allows maximum sensitivity as well as temperature compensation. The gage output was monitored by means of a BLH-120 static strain indicator. In figure 36, the tooth load is plotted versus the strain reading. The input load curve is obtained by hanging weights from the input arm and then reading the strain values. This load is then corrected to give an equivalent load on the gear

Reproduced with permission of the copyright owner. Further reproduction prohibited without permission.

pitch circle. The reaction is obtained by replacing the adjusting screw by a load cell and reading the strain values for various jack input loads. The reaction load is then corrected to an equivalent load on the pitch circle. The tooth load is obtained by replacing the wheel by a lever arm and connecting this arm to the load frame by means of a load cell. The cell output is then obtained for various strain outputs. These steps are shown in figure 37.

The adjusting screw is necessary to allow the gears to be loaded at various angles of rotation. The relative position of the gears is obtained from a pointer mounted on the pinion shaft. The load position is read from a protractor scale.

Reproduced with permission of the copyright owner. Further reproduction prohibited without permission.

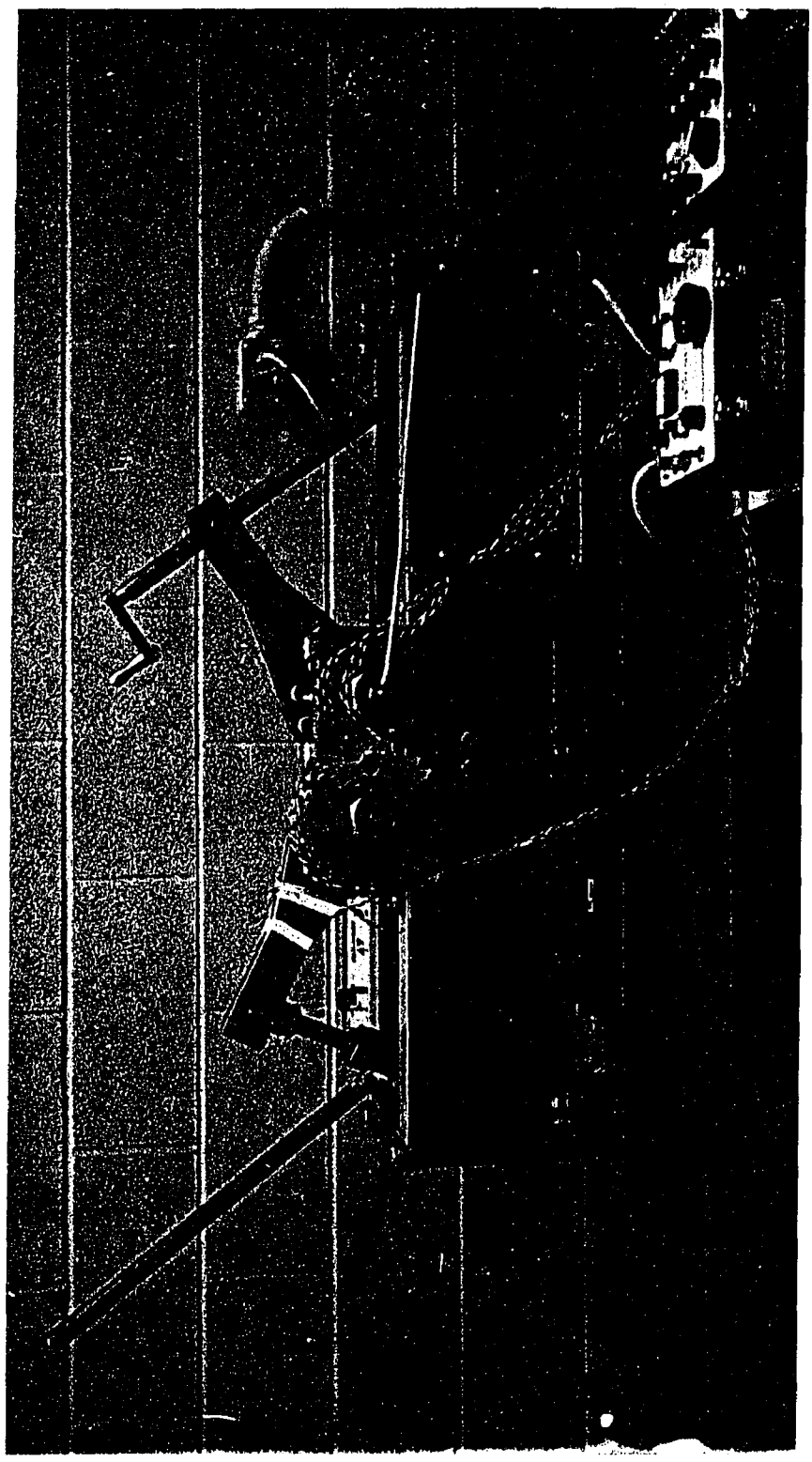

Fig. 35 Gear Loading Frame and Experimental Arrangement

Reproduced with permission of the copyright owner. Further reproduction prohibited without permission.

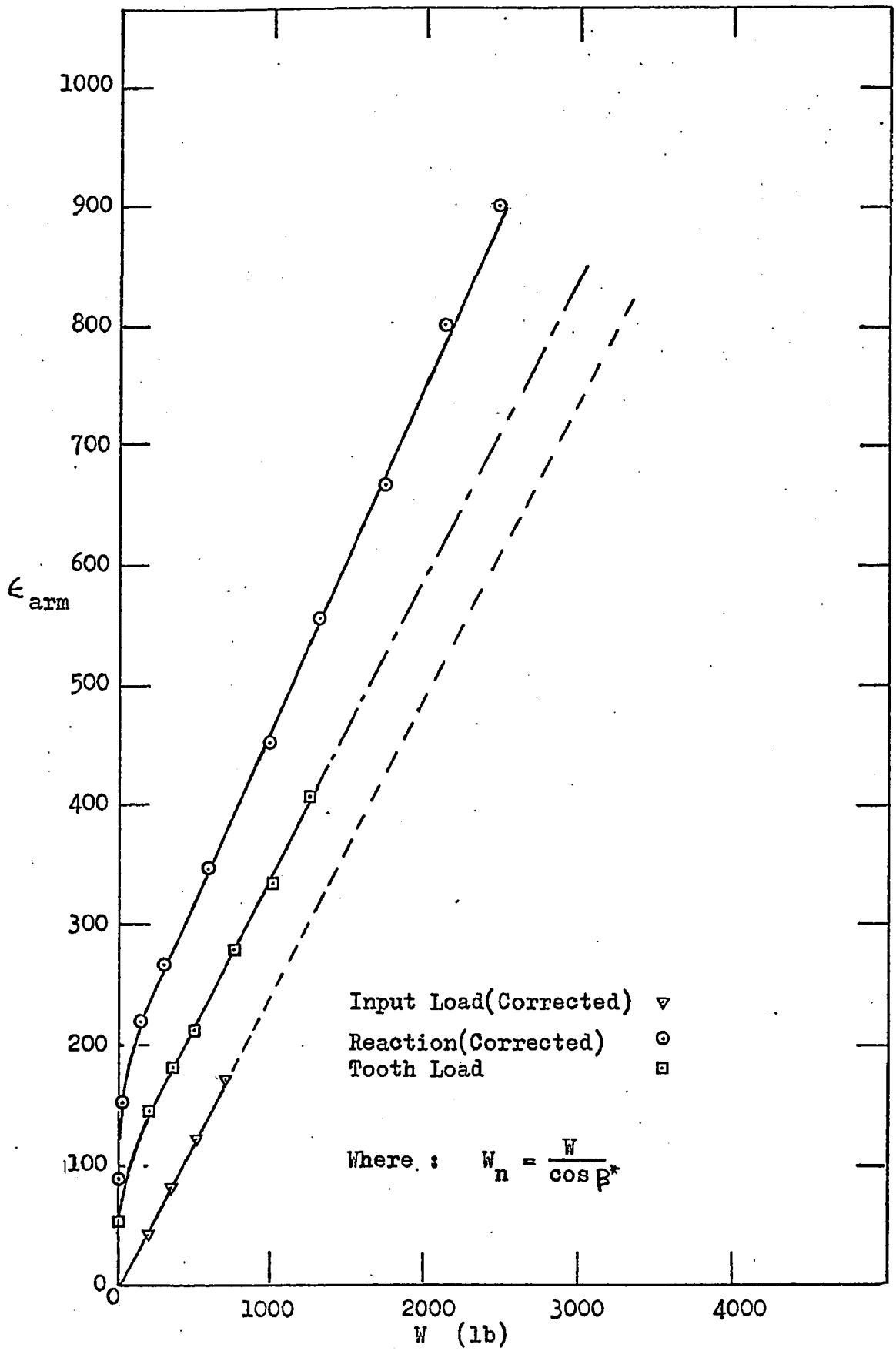

Fig. 36 Tooth Load W vs Strain Reading ϵ_{arm} (μin/in)
Loading Frame Calibration

Reproduced with permission of the copyright owner. Further reproduction prohibited without permission.

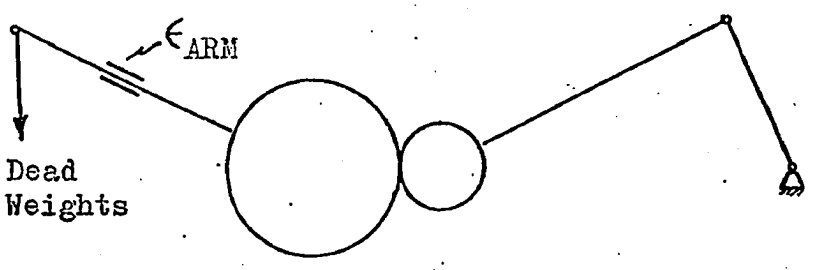

1) Determination of Input

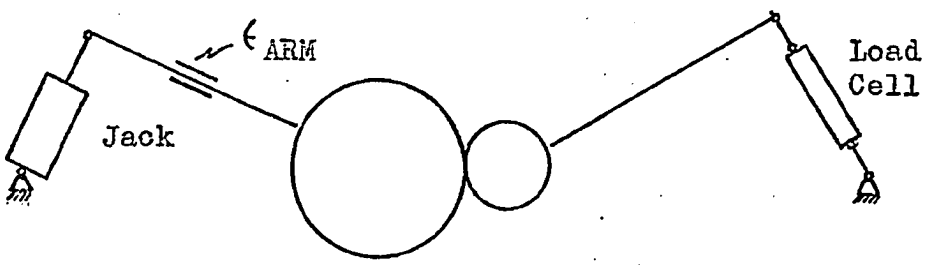

2) Determination of Reaction

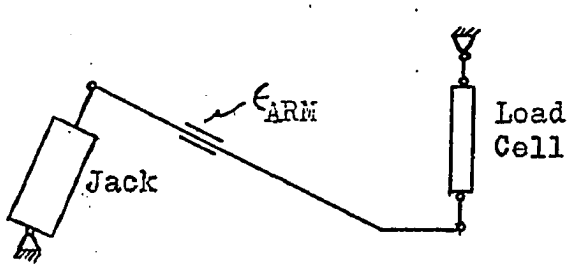

3) Load Determination

Fig. 37 Loading Frame Calibration

Reproduced with permission of the copyright owner. Further reproduction prohibited without permission.

APPENDIX B

PHOTOELASTIC MODEL LOADING APPARATUS

The loading frame was designed to duplicate the actual gear action as is shown in figure 38. This is acheived by fixing the pinion profile against rotation and applying torque through a shaft, which is connected to the wheel profile, by means of a lever arm and dead weights. Accurate centre distance is maintained by means of an adjusting screw which moves the pinion profile with respect to the wheel profile. It is also possible to vary the angle at which the pinion profile is fixed, so that the pitch point can be brought into line with the centres of the two gears.

Reproduced with permission of the copyright owner. Further reproduction prohibited without permission.

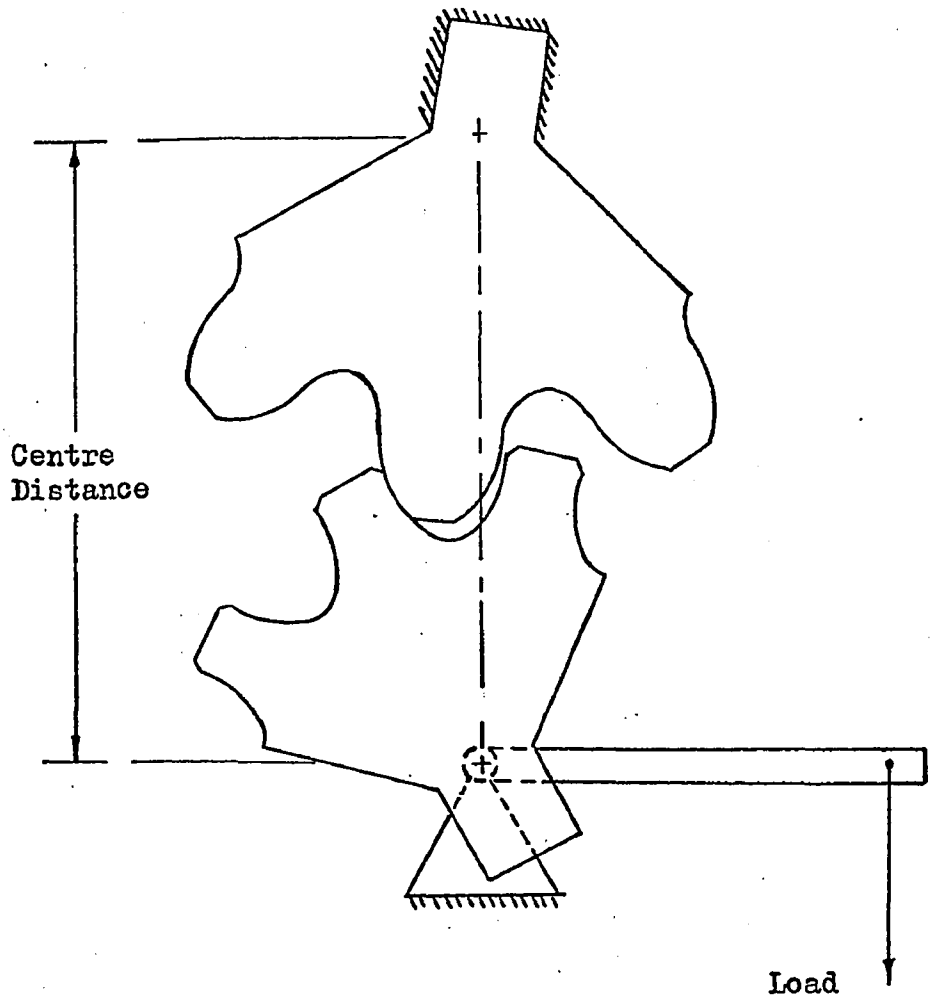

Fig. 38 Photoelastic Loading Frame

Reproduced with permission of the copyright owner. Further reproduction prohibited without permission.

APPENDIX C

LEMMA I

The solution is given for the intersection between two circles with centres (a_1 , b_1) and (a_2 , b_2) and radii r_1 and r_2 .

The equations of the circles are :

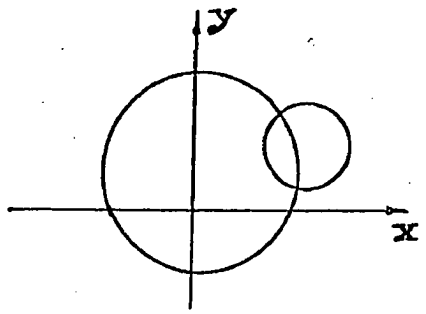

$$x^2 + y^2 - 2a_1x - 2b_1y = r_1^2 - a_1^2 - b_1^2 \quad -①$$

$$x^2 + y^2 - 2a_2x - 2b_2y = r_2^2 - a_2^2 - b_2^2 \quad -②$$

now subtracting ① from ②

$$2x\,(a_2 - a_1) + 2y\,(b_2 - b_1) = (r_1^2 - r_2^2) + (a_2^2 - a_1^2) + (b_2^2 - b_1^2)$$

now define : $A = 2(a_2 - a_1)$

$B = 2(b_2 - b_1)$

$C = (r_1^2 - r_2^2) + (a_2^2 - a_1^2) + (b_2^2 - b_1^2)$

therefore : $Ax + By = C$

or $y = \dfrac{C - Ax}{B} \quad -③$

now substitute ③ into ①

$$x^2\left(1 + \frac{A^2}{B^2}\right) - x\left(2a_1 - 2b_1\frac{A}{B} + 2\frac{AC}{B^2}\right) + \left(\frac{C^2}{B^2} - 2b_1\frac{C}{B} + a_1^2 + b_1^2 - r_1^2\right)$$

then defining :

$$A_1 = 1 + \frac{A^2}{B^2}$$

$$A_2 = 2a_1 - 2b_1\frac{A}{B} + 2\frac{AC}{B^2}$$

$$A_3 = \frac{C^2}{B^2} - 2b_1\frac{C}{B} + a_1^2 + b_1^2 - r_1^2$$

Reproduced with permission of the copyright owner. Further reproduction prohibited without permission.

then $A_1x^2 - A_2x + A_3 = 0$

therefore

$$x = \frac{A_2 \pm \sqrt{A_2^2 - 4A_1A_3}}{2A_1}$$

LEMMA II

The solution is given for the points of tangential intersection between a circle and a parabola symmetric about the y axis with its vertex at the origin .

The equations are :

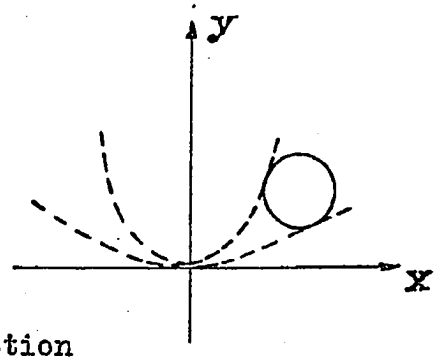

$$(x - a)^2 + (y - b)^2 = r^2 \quad - ①$$

$$y = kx^2 \quad - ②$$

In order to have tangential intersection the slopes of the two curves must be equal at the intersection point .

therefore $$2kx = -\frac{x - a}{y - b} \quad - ③$$

now substitute ② in ③

$$x^2 + 2y^2 - ax - 2by = 0 \quad - ④$$

rewriting ①

$$x^2 + y^2 - 2ax - 2by = -c^2$$

where $c^2 = a^2 + b^2 - r^2$

now subtract ① from ④

$$y^2 + ax = c^2$$

Reproduced with permission of the copyright owner. Further reproduction prohibited without permission.

therefore $x = \frac{c^2 - y^2}{a}$ - ⑤

now substitute ⑤ in ④

$$y^4 + (a^2 - 2b^2 + 2r^2) - 2a^2by + (a^2 + b^2 - r^2)(b^2 - r^2) = 0$$

this fourth order equation must be solved for the value of y of interest .

Reproduced with permission of the copyright owner. Further reproduction prohibited without permission.

APPENDIX D

PHOTOSTRESS MATERIAL CALIBRATION

The photostress used was a polyester resin obtained from Photolastic Incorporated under the code name PSM-1A. It was attached to the calibration model employing a reflective epoxy cement.

The calibration model was an aluminum ring (6061-T6), with inner diameter 3 inches, outer diameter 5 inches and thickness $\frac{1}{2}$inch. The photostress thickness was 1/8 inch, which was the same as that used on the metal gears, (see figure 39).

Figure 40 shows the theoretical and experimental stress variation with load. The experimental values were obtained using strain gages at the points indicated. Figure 39 shows the fringes which occur in the model under test, while figure 41 shows the variation with load of the fringes at the two positions shown. The values do not go to zero because of residual stress in the model edge.

It is possible to calculate the fringe constant from this information as K= .157. The value given by the manufacturer was 0.15.

Relating this to the steel gears shows that it takes 13500 psi to produce one fringe in the photostress.

The detailed calculations are as follows:

ring thickness = .500 inches

Photostress thickness = .126 inches

Therefore the correction factor C = 0.99

The stress to fringe order relationship is

$$\sigma_1 - \sigma_2 = \frac{\lambda N}{2 t_p K C} \times \frac{E_s}{1+\mu_s}$$

where λ = wave length of light used = 22.7×10^{-6} inches

N = fringe order

t_p = thickness of plastic

K = fringe constant

C = correction factor

E_s = modulus of elasticity of ring = 10×10^6 psi

Reproduced with permission of the copyright owner. Further reproduction prohibited without permission.

μ_s = poissons ratio of ring = 0.33

σ_2 = 0 at the boundary of the ring

now $\frac{\sigma}{N} = \frac{\sigma}{P} \times \frac{P}{N}$

P/N can be obtained from figure 40

σ/P can be obtained from figure 39

then $\sigma/N = 4.62 \times 10^3$

from this K = .157

Reproduced with permission of the copyright owner. Further reproduction prohibited without permission.

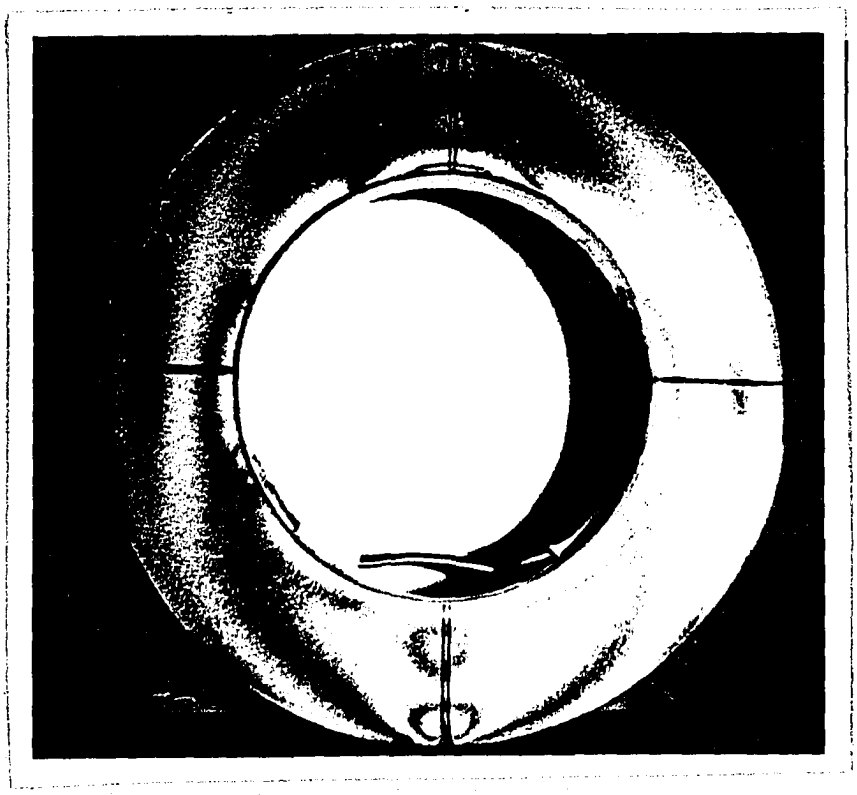

Fig.39 PSM-1 Calibration Ring : Load = 1150 lb.
Isochromatic Fringe Photograph
(Reflection Polariscope)

Reproduced with permission of the copyright owner. Further reproduction prohibited without permission.

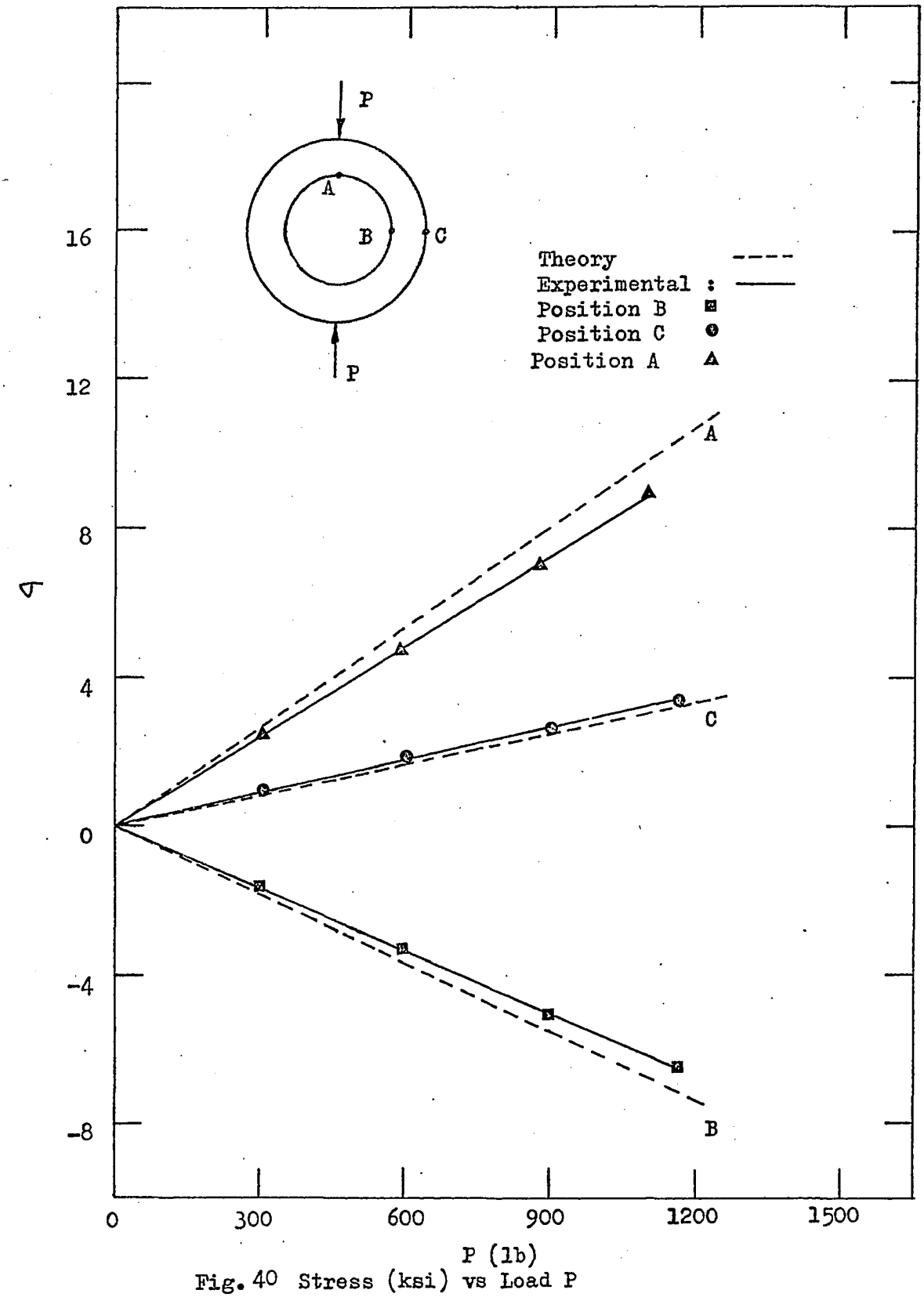

Fig. 40 Stress (ksi) vs Load P

Reproduced with permission of the copyright owner. Further reproduction prohibited without permission.

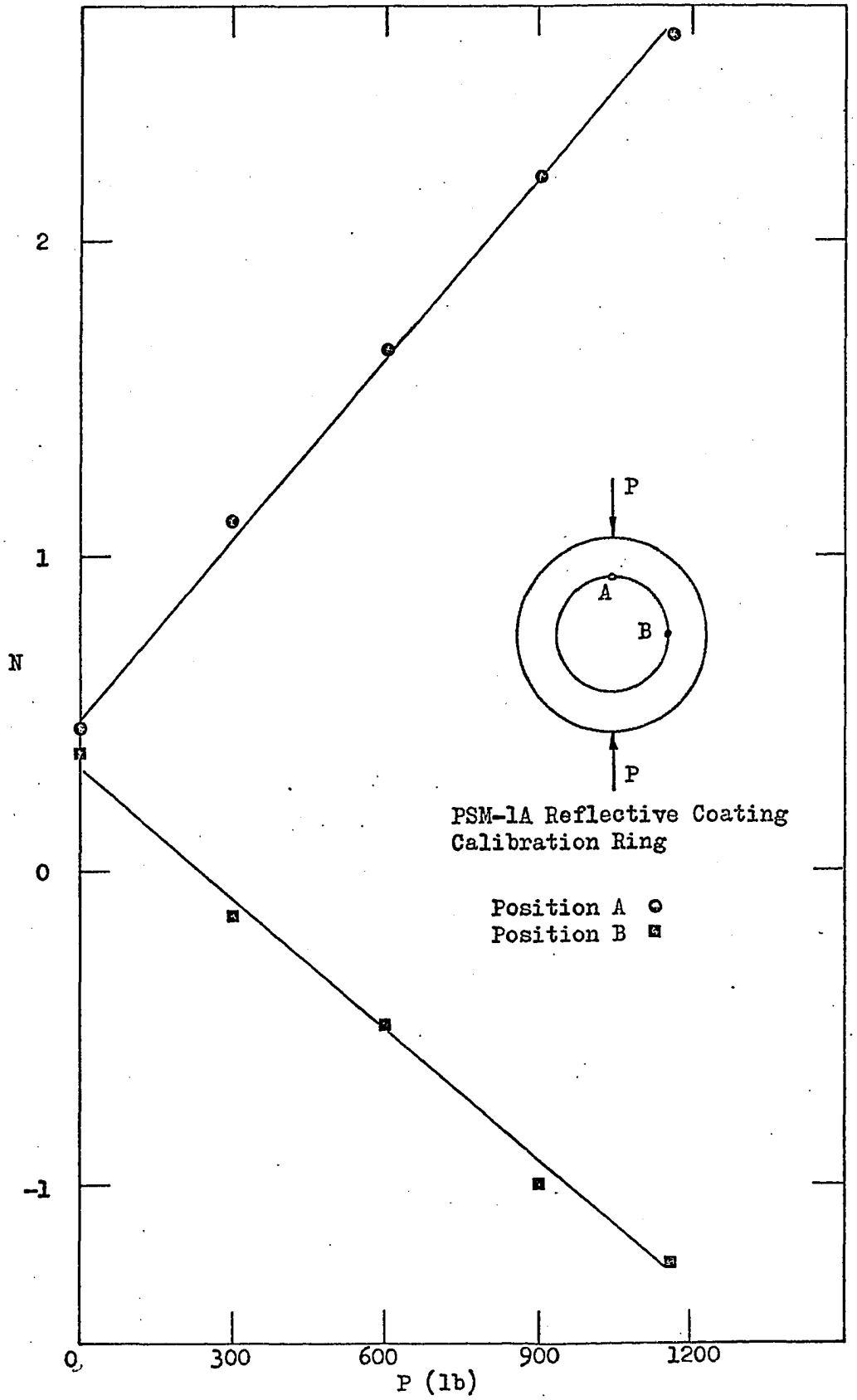

Fig. 41 Fringe Order N vs Load P
For Green Light

Reproduced with permission of the copyright owner. Further reproduction prohibited without permission.

APPENDIX E

PHOTOELASTIC MATERIAL CALIBRATION

The material used in this study was a polyester material called PSM-1, obtained from Photolastic Incorporated. This material exhibits low creep, excellent time edge effects and ease of machining. The given material specifications were:

Poisson's Ratio (γ) 0.38

Modulus of Elasticity 340,000 psi

Material fringe constant 40 psi-in./fringe (nominal)

The material was calibrated by cutting a constant moment beam from the same batch of material as the tooth profiles and plotting the fringe order versus edge stress as seen in figure 42. The fringe order is seen to be linear to at least twenty fringes. The material constant is then calculated from the slope of this curve as 37.8 psi-in./fringe.

The detailed calculations are:

beam thickness = 0.255 inches

beam depth = 0.750 inches

distance between load points = 1.00 inches

$$\sigma = \frac{Mc}{I}$$

M = bending moment = P lb-in.

c = distance to neutral axis = 0.375 inches

I = moment of inertia = .00898 $in.^4$

therefore $\sigma = \frac{.375\,P}{.00898} = 41.7\,P$ psi

then knowing the applied load (P) we may obtain the stress.

From figure 41 we see that $\sigma/N = 146.5$ psi/fringe.

The stress optic law states that

$$\sigma_1 - \sigma_2 = \frac{Nf_\sigma}{h}$$

At the point studied $\sigma_2 = 0$ (free boundary)

therefore $f_\sigma = 37.8$ psi-in./fringe

Reproduced with permission of the copyright owner. Further reproduction prohibited without permission.

The models (both the calibration beam and the gear profiles) were made of $\frac{1}{2}$ inch thick material (nominal) and were machined to final shape employing a metal template as a guide. The machining process was carried out employing a four fluted end mill in a modified drill press. The machining was done in stages with the depth of cut being increased with each pass of the cutter. Final finishing of the two contact areas was accomplished using fine emery paper and very light passes. This process was found necessary to improve contact stresses between the two contacting surfaces.

Reproduced with permission of the copyright owner. Further reproduction prohibited without permission.

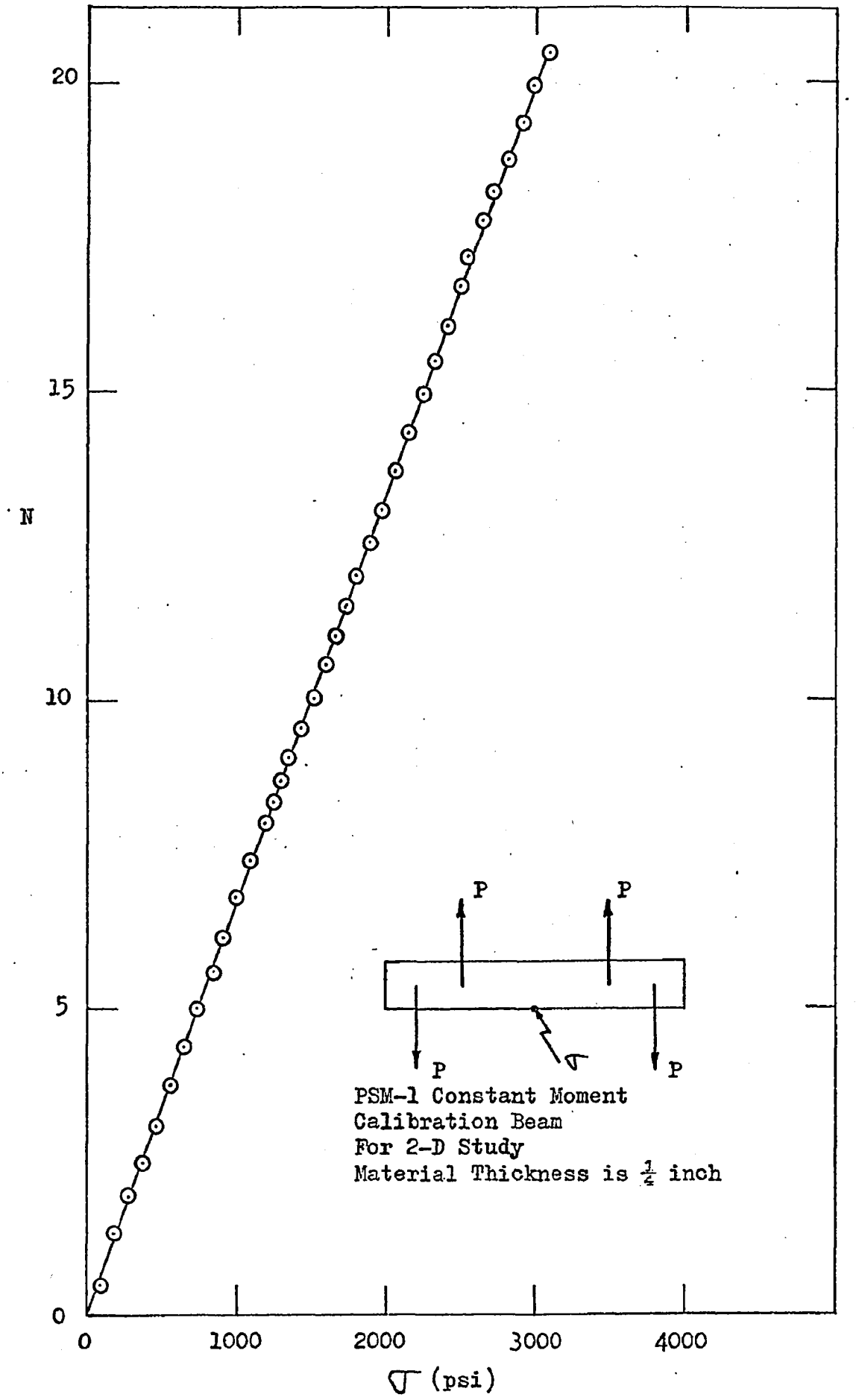

Fig. 42 Fringe Order N vs Stress

Reproduced with permission of the copyright owner. Further reproduction prohibited without permission.

APPENDIX F

COMMERCIAL EQUIPMENT USED

1) BLH Strain Indicator, Model 120
2) Budd P350 Strain Indicator
3) Budd Switch and Balance Unit, Model SB-1
4) Budd LF/M Photostress Meter
5) Budd Telemicroscope attachment for LF/M equipped with a Sun Zoom Lens (85-210 mm.)
6) Nikkormat FTN, 35 mm. camera
7) Tinius Olsen, 6000 lb. capacity, testing machine
8) Bellows extension camera with a 4 x 5 cut film back
9) Strain Gages
   a) Used on gear teeth
      BLH type FAE-03S-12S6
      Serial # 2-A-GK Lot # 257
      Resistance = 120.0 $\pm$ .2 Ω
      k = +0.1%
      G.F. = 1.88 $\pm$ 2%
   b) Used to monitor input load
      BLH type FA-50-12S6
      Resistance = 120.0 $\pm$ .2 Ω
      k = + .2%
      G.F. = 2.09 $\pm$ 2%
   c) Used on ring for photostress calibration
      Micro Measurements
      EA-13-250BG-120
      Resistance = 120.0 $\pm$ 0.5% Ω
      G.F. = 2.09 $\pm$ 0.5%
      K = + 0.5%
      Lot number Q-A18AF09

Reproduced with permission of the copyright owner. Further reproduction prohibited without permission.

VITA

1944 Born in Stekene, Belgium

1967 Received the Degree of Bachelor of Applied Science in Mechanical Engineering from the University of Windsor, Windsor, Ontario .

1969 Presently a candidate for the Degree of Master of Applied Science in Mechanical Engineering at the University of Windsor, Windsor, Ontario .

Reproduced with permission of the copyright owner. Further reproduction prohibited without permission.